Polymer Journal, Vol. 38, No. 7, pp. 611–638 (2006)

AWARD ACCOUNTS: SPSJ MITSUBISHI CHEMICAL AWARD (2005)

Several Interesting Fields Exploited through Understanding of Polymeric Effects on Liquid Crystals of Main-Chain Polyesters

Masatoshi TOKITA and Junji WATANABE†

Department of Organic and Polymeric Materials, Tokyo Institute of Technology, Ookayama, Meguro-ku, Tokyo 152-8552, Japan

(Received April 10, 2006; Accepted May 1, 2006; Published June 20, 2006)

ABSTRACT: We review our experimental results on the structural characteristics of polymeric liquid crystals collected through our studies on the main-chain liquid crystalline polyesters with mesogenic biphenyl groups connected by flexible alkyl spacer. The polyesters studied, designated as BB-*n* where *n* is the number of carbon atoms in the alkyl spacer unit, form smectic mesophases. Of interest is that the type of smectic phase alters depending on the odd-even parity of *n*. An ordinal smectic A phase is formed by BB-*n* with even *n*, whereas BB-*n* with odd *n* forms a new type of smectic phase, so called smectic CA phase, in which the long axis of the mesogen is tilted against the layer normal and the tilting direction is opposite between neighboring layers. Finding of smectic CA phase with specific packing symmetry leads to a distinct discovery of ferroelectric and antiferroelectric phases in achiral molecular systems. In these smectic phases, the polymer chain assumes more extended conformation. Such an extended conformation, however, does not continue over the whole length of the polymer and hairpin folding arises to gain entropy. In the smectic phases, the hairpin foldings are located at a limited space, forming chain folded lamellae. Unusual shear flow orientation and anomalous crystallization behavior are explained based on the chain folded lamellar structure. Solid state morphology of liquid crystalline polymer is also presented. Since the degree of liquid crystallinity is almost 100%, the solid phase cooled through the formation of liquid crystals is composed of crystal and liquid crystal glass. Liquid crystal glass is studied and properties are discussed in a comparison with those of conventional isotropic glass.
[doi:10.1295/polymj.PJ2006008]

KEY WORDS Liquid Crystalline Polymer / Smectic Phase / Smectic CA / Ferroelectric Phase / Chain Folding / Chain Folded Lamella / Nematic Elastomer / Liquid Crystal Glass /

Molecular structures of liquid crystalline polymers are usually characterized in terms of locations of mesogenic groups. In the main-chain liquid crystalline polymers, the mesogenic groups within a polymer backbone are linked to each other through a flexible spacer. Each mesogenic group forms mesophase structure as in the low-molecular-weight materials, but the polymer molecules must adopt a conformation or packing compatible with the structure of mesophase. As a result, mesogenic properties are closely coupled with the polymeric properties. Considering that the polymer chain conformation is dominated by the conformation of flexible spacer, alteration of the flexible group may influence the molecular packing into a mesophase and result in the structure and properties which depart from those of the low-molecular-weight mesogen. In this paper, focusing on this coupling effect, we review our experimental results on the structural characteristics of polymeric smectic liquid crystals which have been collected through our studies on the main-chain liquid crystalline polyesters with the biphenyl group as a common mesogen.[1–24]

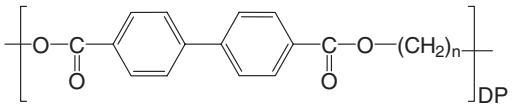

The polyester is designated as BB-*n* where *n* is the number of carbon atoms in the alkyl spacer unit.

The paper is edited as follows. The first section refers to the odd-even effects on smectic properties and structures in the BB-*n* polyesters. In these polymers, alkyl spacer assumes the more extended conformation that is coupled with the cooperative orientation of mesogenic groups, but its conformational constraint appears different between the odd and even-numbered polymers. As a result, a new type of smectic CA phase is formed from the odd-membered BB-*n* polyesters. In the second section, the structural details of new smectic CA phase are presented. The third section shows that new types of ferroelectric and antiferroelectric liquid crystals can be designed in achiral system based on the polymeric effects clarified in the preceding sections. The forth section addresses the problem on the polymer chain configuration, *i.e.*, whether the polymer chains are extended along the entire length or not in

†To whom correspondence should be addressed (E-mail: jwatanab@polymer.titech.ac.jp).

the smectic liquid crystalline field. In the final section, we describe the characteristics of smectic liquid crystal glass.

ODD-EVEN EFFECTS ON SMECTIC PROPERTIES AND STRUCTURES

The BB-*n* polyesters with *n* of 3 to 9 exhibit two transitions in DSC thermograms.[1,2] Thermodynamic data of BB-*n* polyesters based on DSC are given in Figures 1a and 1b. Figure 1a shows variation of the transition temperatures with *n*. Here, one can find a simple trend that the mesophase temperature region decreases with increase of *n* and finally the mesophase disappears when *n* exceeds 10. The isotropization entropies of liquid crystals are given in Figure 1b. Figures 1a and 1b indicate the clear odd-even oscillation with the larger value observed in even-membered BB-*n* polyesters.

The mesophases observed here can be assigned to the smectic phase from the X-ray observation of the sharp inner layer reflection and the outer broad reflection and also from the microscopic observation of the fan-shape texture. The spacings of inner reflection, *i.e.*, the smectic layer thicknesses, are plotted against *n* in Figure 2. One can also observe the odd-even oscillation with a larger spacing in the even-membered BB-*n* polyesters.

The most striking feature in this system is that the type of smectic phase appears different depending on the odd-even parity of *n*. This was initially shown by X-ray observations of the oriented fiber specimens spun from the isotropic melt.[3] Figures 3a and 3b show the X-ray diffraction patterns of the oriented smectic phases of BB-6 and BB-5, representative materials of even- and odd-membered polymers, respectively. In BB-6, as found in Figure 3a, the layer reflections are located on a meridional line and the broad reflections are on an equatorial line. This diffraction geometry unambiguously indicates a smectic A (S_A) structure in which the mesogenic groups forming a layer are arranged parallel to the polymer chain and both lie perpendicular to the layers (see Figure 3c and Figure 4a). The BB-5 polyester shows distinct X-ray

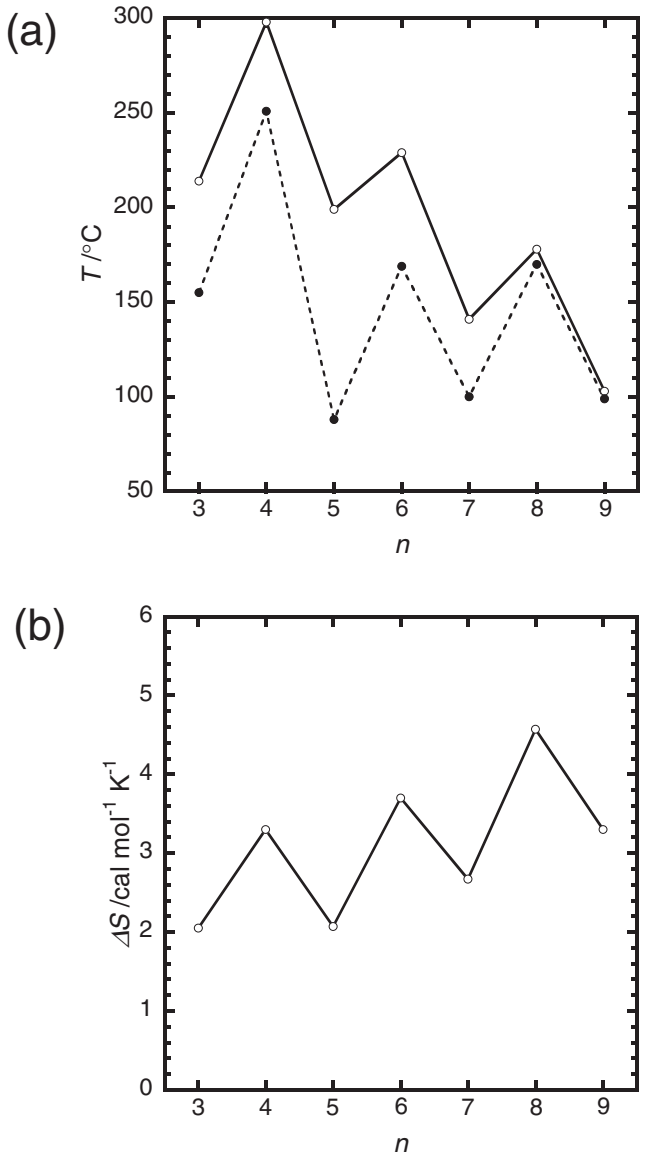

Figure 1. Variation of (a) transition temperatures (●, for the crystal to liquid crystal transition; ○, for isotropization of liquid crystal) and (b) isotropization entropy of liquid crystal, with the carbon number of alkylene spacer, *n*.

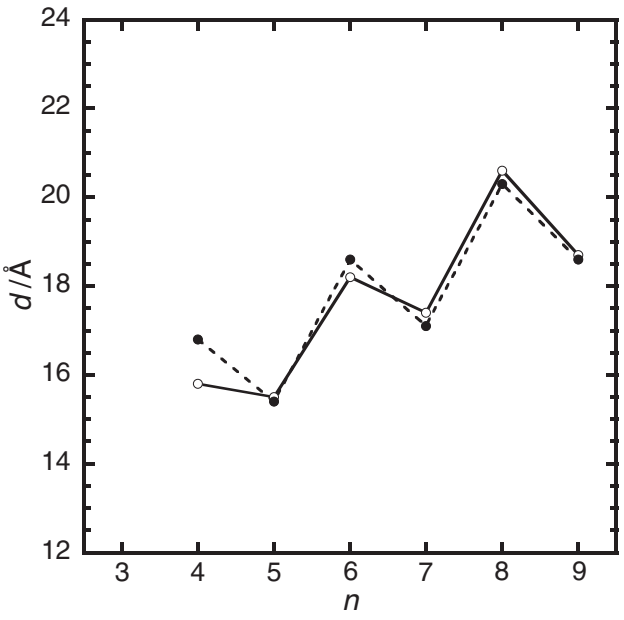

Figure 2. Variation of the smectic layer thickness (open circle) with *n*. Here, the closed circle shows the calculated layer thickness which corresponds to the distance between the mesogenic groups averaged over the confined conformers with the small angular displacement of successive mesogens (refer to the text and Figure 5).

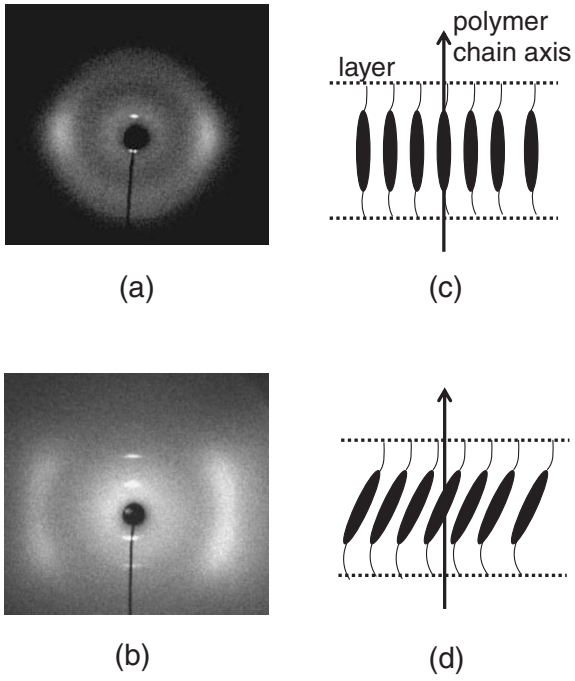

Figure 3. Oriented X-ray pattern taken for the fibrous smectic phases of (a) BB-6 and (b) BB-5. The packing structures of mesogenic groups within a layer elucidated from the X-ray patterns are also illustrated in (c) and (d). Here, the oriented fibers were prepared by pulling the isotropic melt and the fiber axis is placed in the vertical direction.

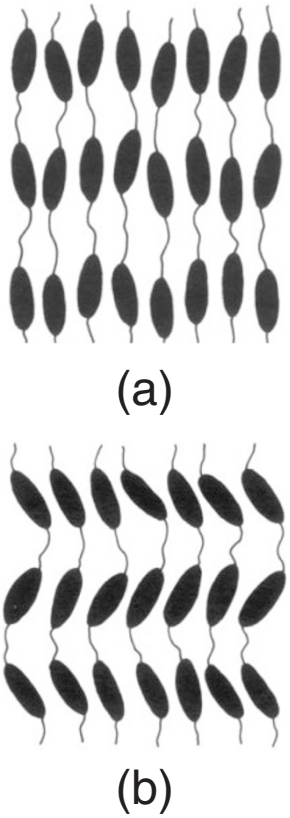

Figure 4. Layered structures of the smectic phases of (a) BB-6 and (b) BB-5.

pattern shown in Figure 3b. The broad outer reflections are split into two portions lying above and below the equator while the layer reflections appear on a meridional line as in BB-6.[2,6] In this case, the layered packing structure can be illustrated such that the polymer chains lie perpendicular to the layer as in BB-6 but the mesogenic groups are tilted to the layer normal (see Figure 3d). Tilt angle is independent of temperature and elucidated about 25° from the splitting angle of the broad reflections.[2] The structure is thus similar to the smectic C (S_C) as far as the arrangement of mesogenic groups within a layer is concerned.

To account for this odd-even oscillation in the smectic structures, conformational analysis of the flexible spacer has been performed within a framework of the rotational isomeric state model, and evaluated the angle θ, defined by unit vectors attached to two successive mesogenic groups.[12,25] The results are shown in Figure 5 where the relative numbers of conformers are plotted against θ for BB-6 and BB-5. From this figure, we see that the angular distributions are completely different between the even- and odd-series of BB-*n* polymers. When *n* is even, the angles θ are found to be distributed in two ranges of 0 to 20° and 90 to 120°. For odd *n*, most of the angles are located in the region of 50 to 90° and to some degree orientation is also permitted in the region above 150°. In each system, the conformers with the smaller angular displacement of successive mesogens are in the more extended form. Based on this calculation, we can arrive at the following points which are closely related to the observed characteristics in the smectic layered structures.[12,25]

(1) In the n = even series the parallel orientation of successive mesogenic groups is allowed, conforming more or less to the concept of an ordinary uniaxial ordering of the n-director, but in the n = odd series uniaxial orientation of successive mesogenic groups is not allowed (see Figure 5).

(2) The conformers with the smaller angular displacement in both odd and even systems correspond to the conformers participating in the observed layer structure (compare Figure 4 with Figure 5).

These explain the odd-even appearance in the type of smectic phases and at the same time, suggest the specific formation of a distinct smectic phase in the odd-numbered BB-*n*, leading to the significant conclusion that the structure of smectic phase is strongly promoted by the conformational constraint of a flexible spacer. This conclusion is supported by a comparison of the observed layer thickness with the calculated layer thickness,[12] which corresponds to a distance between the neighboring mesogens in a chain. As found in Figure 2, the absolute value as well as the odd-even oscillation can be perfectly reproduced when the cal-

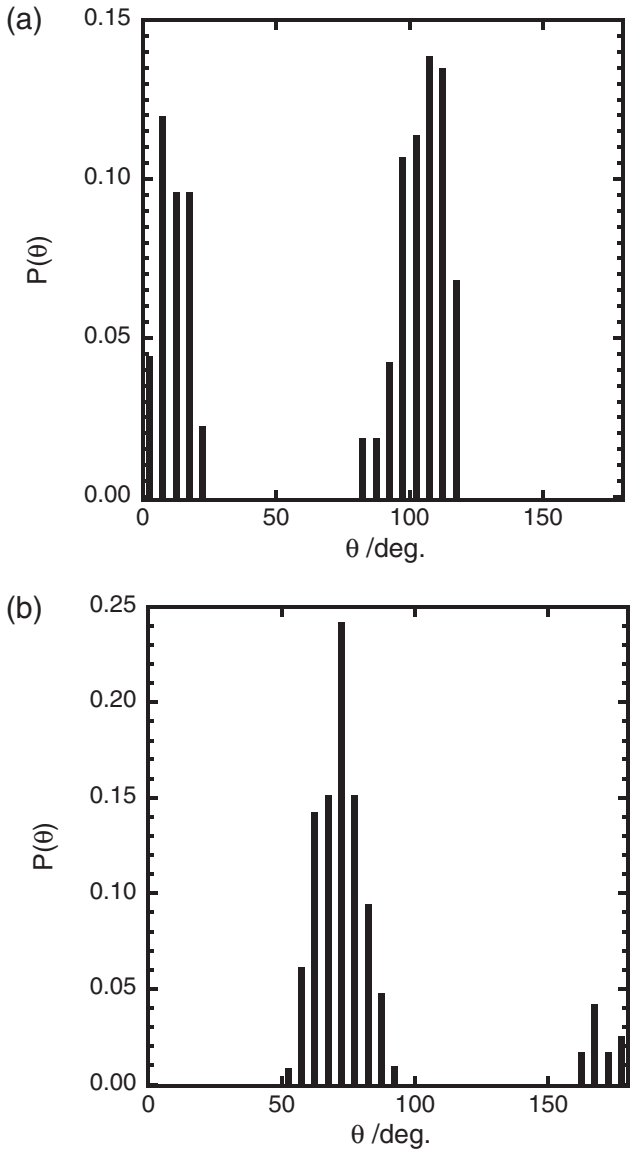

Figure 5. Distribution of chain conformer calculated for the angle θ defined by two successive mesogens; (a) BB-6 and (b) BB-5. The rotational angles and statistical weights in Table II of reference 25 are adopted for the calculation.

culation was performed for the confined conformers with the smaller angular displacement.

DISTINCT SMECTIC CA PHASE

From the above, it is strongly suggested that the odd-membered BB-*n* polyesters form the distinct smectic phase, as illustrated in Figure 4b, in which the polymer chains are perpendicular to the layer but the mesogenic groups are tilted to the layer in an alternate fashion. In most types of liquid crystals so far observed, uniaxial orientation is for the long axes of mesogens. In this sense, the smectic phase suggested here is quite novel and interesting since uniaxial ordering cannot be observed for n-director but only for the c-director.[6] This smectic phase is designated as smectic CA (S_{CA}) phase.[26] This section presents experimental evidences for the formation of the quite novel S_{CA} phase in odd-membered BB-*n* polyesters.

Optical Texture Characteristic of S_{CA}

Evidence for the S_{CA} structure is the observation of dispiration in homeotropically arranged sample.[6] Its typical homeotropic textures as observed in BB-5 are given in Figures 6b and 6c. High birefringence and also various schlierens can be observed. These observations, together with the X-ray observations, undoubtedly show that the c-director exists in each layer and its orientation correlation is maintained from the layer to layer. To be emphasized here is that the schlieren texture with singularities of $s = \pm 1/2$ is observed in this smectic phase (see Figure 6c). This fact rules out the assignment to a S_C phase[27] and leads to only a S_{CA} structure of Figure 4b.[6–8] Figure 7 illustrates the c-director alignment to produce the $s = \pm 1/2$ disclination in the S_{CA} phase. Here, the edge disclination is coupled with helical dislocation, that is, one layer shifts to its neighboring layer after a rotation of 180° around disclination line. This combined effect with edge disclination and helical dislocation is called a dispiration.[28] Thus, the odd-numbered BB-*n* sample allows the first visual observation of the dispiration as well as the discovery of S_{CA} structure.[6–8]

Unique Helical Structure in Chiral Smectic CA Phase

Other evidence for the S_{CA} structure is given by a characteristic helical structure which results from the helical twisting of c-director in its chiral phase. The chiral S_{CA} phase can be attained in the BB-3*(1-Me) polyester with the chiral 1-(s)-methyl propyl unit as a flexible spacer as given below.[6]

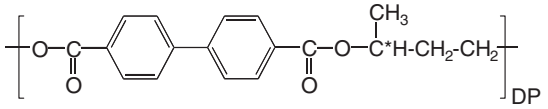

Since the S_{CA} phase has an alternate tilting of mesogenic groups in successive layers, *i.e.*, the two different sets of c-director vectors, the resultant helical structure should be essentially different from that of the conventional chiral S_C which has only a set of c-director vector. In other words, it can be regarded as identical to two chiral S_C helices geared into each other with a phase difference of π. In Figure 8, such a peculiar helical structure is schematically illustrated and compared with the helical structure of chiral S_C.

Such a difference in a helical structure between the chiral S_{CA} and S_C can be confirmed through the selective reflection property of light. On this point, we first

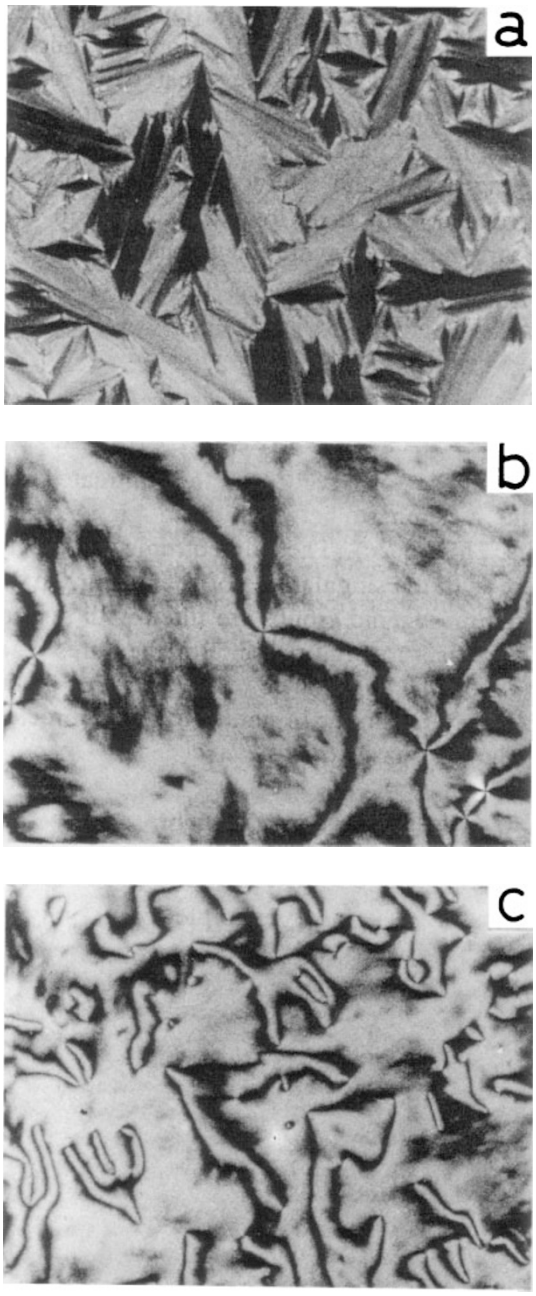

Figure 6. Optical microscopic textures observed for the smectic phase of BB-5. a): The fan-shape texture observed for the untreated specimen prepared by slow cooling from isotropic melt. b) and c): Homeotropic textures for the specimens which were prepared by shearing between glasses. Homeotropic textures are birefringent and include the schlierens with point singularities of $s = 1$ (b) and $s = 1/2$ (c).

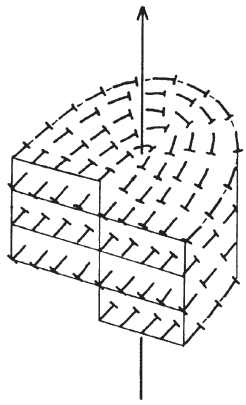

Figure 7. c-Director orientation around the wedge dispiration with rotational component of π which can be expected for the S_{CA} phase. The translational component gives rise to the step.

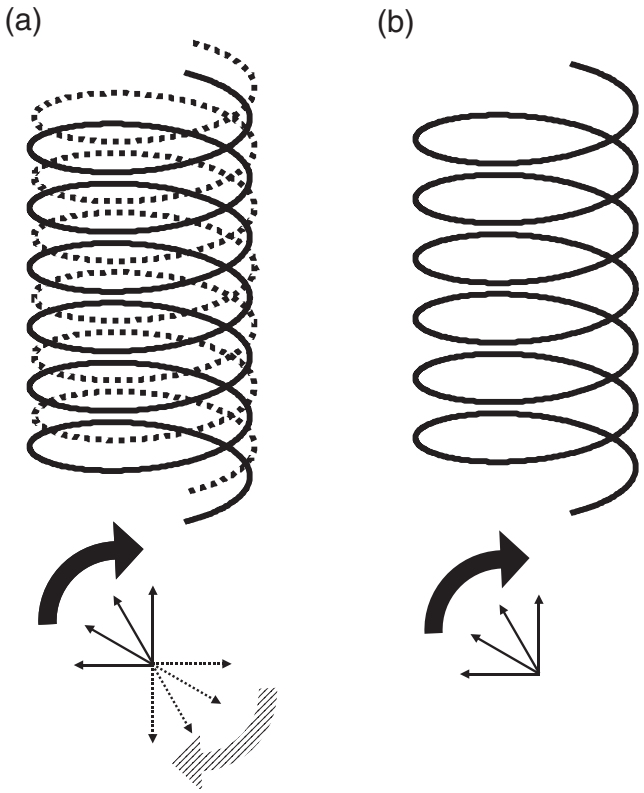

Figure 8. Schematic illustration of the arrangement of the c-directors in (a) chiral S_{CA} and (b) chiral S_C phases.

try to figure out the helical arrangement of the refractive index ellipsoids. In both smectic phases, the index ellipsoid has a biaxial nature, as illustrated in Figure 9. In the S_{CA} phase, the unit cell includes two layers and molecular packing has a crystallographic D_{2h} symmetry.[6,29] Hence, the z-axis giving maximum refractive index lies perpendicular to the layers as illustrated in Figure 10a. In the S_C with C_{2h} symmetry, in contrast, the corresponding z-axis is tilted to the layer plane (see Figure 9b). Since the helical structure is formed along the layer normal, there should be remarkable difference in helical arrangement of index ellipsoids between both phases. Shown in Figure 10 is such a different situation. In a helix of chiral S_C, the index ellipsoid rotates around the helical axis with a certain tilting of z-axis while in helical chiral S_{CA}, it rotates keeping the z-axis parallel to the helical axis.

Let's irradiate light on these two helices. When the light propagates parallel to the helical axis, both phas-

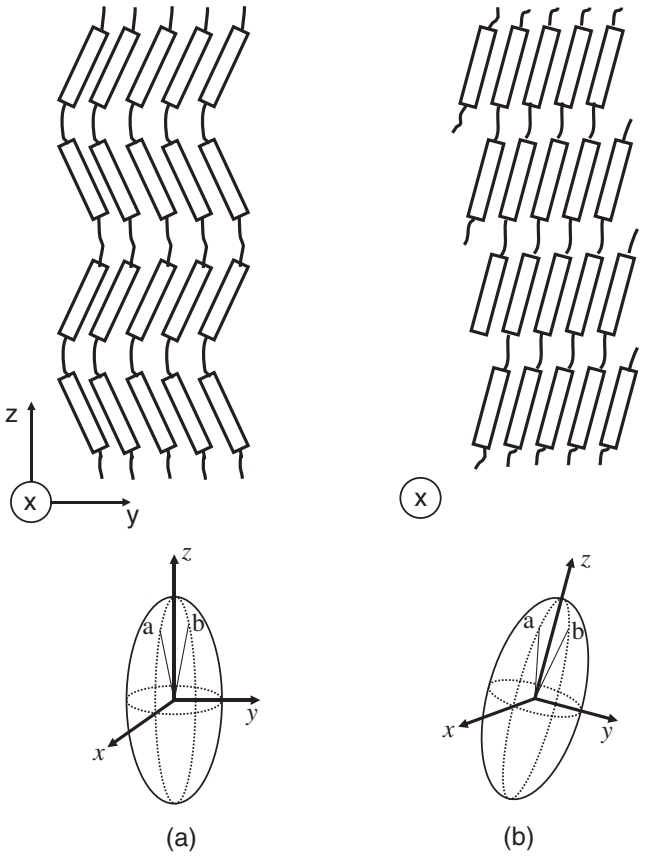

Figure 9. Molecular ordering and optical index ellipsoid in (a) the S_{CA} and (b) S_C phases.

es exhibit the selective reflection of the light with the wavelength equal to a half pitch, since the layer giving the same refractive indices appears in every half pitch. Such a reflection band is called here a half-pitch band. In contrast to this, when the light propagates in a tilted direction to the helix axis, the same refractive indices no more appear in every half pitch for the chiral S_C but in every full pitch, while in the chiral S_{CA} they still repeat in every half pitch. On tilted irradiation of light to the helix axis, the chiral S_C should newly show a full-pitch band while the chiral S_{CA} should still exhibit only a half-pitch band like a cholesteric phase.[30,31]

The experimental evidence for these reflection properties is given in Figure 11.[6] With irradiation of light parallel to the helix axis, only a half pitch band can be observed for both chiral phases. By tilted irradiation (for example on 60° irradiation), in contrast, the full pitch band appears in chiral S_C but not in chiral S_{CA}. The results are thus obtained as expected, confirming again the structural peculiarity of S_{CA} phase.

Biaxiality in S_{CA} Structure Evidenced from X-ray Patterns of Thin S_{CA} Film

Here, we refer to distinct molecular orientation observed in a thin film of S_{CA} phase where the zigzag tilting of mesogenic groups takes place preferentially

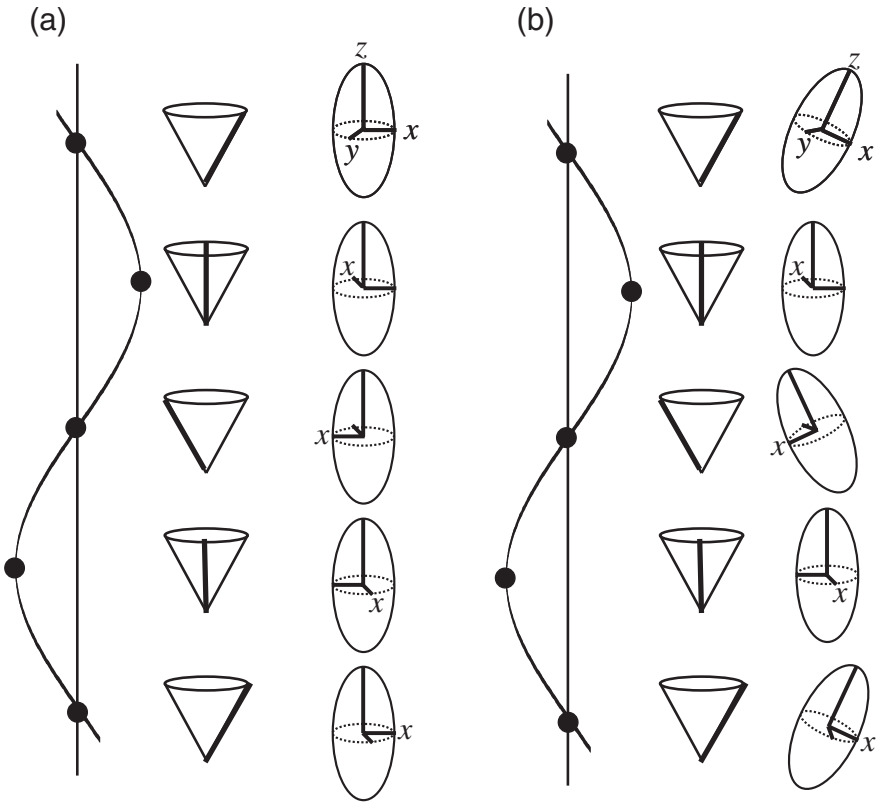

Figure 10. Schematic illustration exhibiting helical arrangement of the refractive index ellipsoids in (a) the chiral S_{CA} and (b) chiral S_C phases.

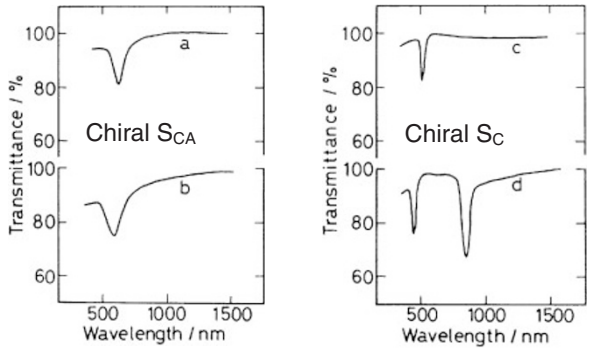

Figure 11. Reflection spectra for chiral S_{CA} and chiral S_C phases with homeotropic alignment. (a) and (c); the reflection spectra as measured by the incident light parallel to the helix axis. (b) and (c); the reflection spectra as measured on incidence inclined by 60° to the helix axis.

in a direction perpendicular to the film surface. This is also a clear evidence for the biaxiallity of S_{CA} phase.[20]

The polymer used here is BB-$(OEt)_2$ with the following structure,

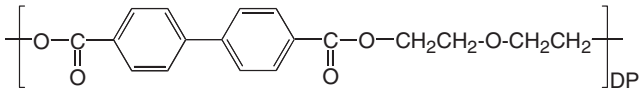

that belongs to the odd homologue of polymers since the number of atoms in the spacer is five. BB-$(OEt)_2$ shows a S_{CA}-isotropic transition at 199 °C on heating and at 180 °C on cooling. No crystallization took place at a normal cooling rate. Oriented film with a thickness of around 20 μm was prepared by stretching the viscous isotropic melt at a high rate of around 1 cm s^{-1}. Figures 12(a)–(c) show its X-ray patterns

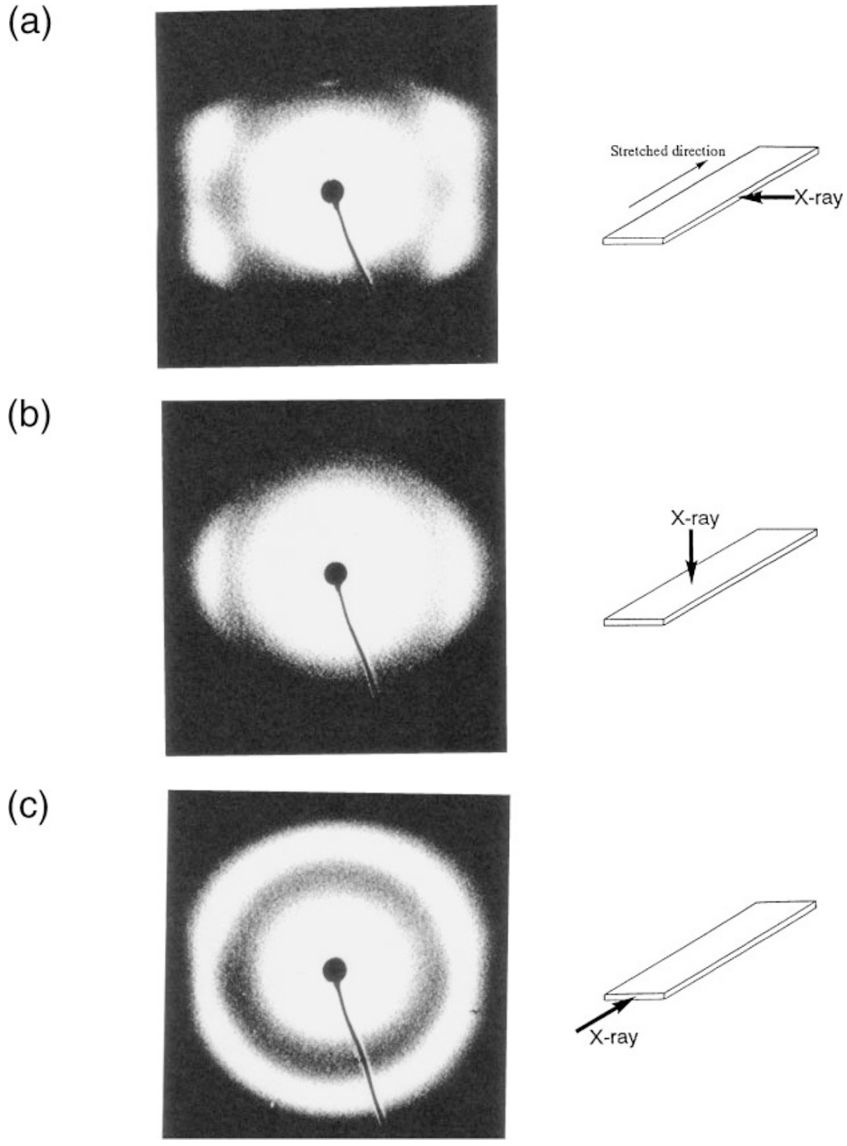

Figure 12. X-ray diffraction patterns for the oriented S_{CA} film of BB-$(OEt)_2$ taken by irradiation from three characteristic positions. Thin film with a thickness of around 20 μm was prepared by stretching the isotropic melt and the X-ray beam was irradiated (a) parallel to the film surface and perpendicular to the chain axis, (b) perpendicular to the film surface, and (c) parallel to both the film surface and chain axis. In (a) and (b) the chain axis is placed in the vertical direction, and in (c) the film surface is parallel to the horizontal direction.

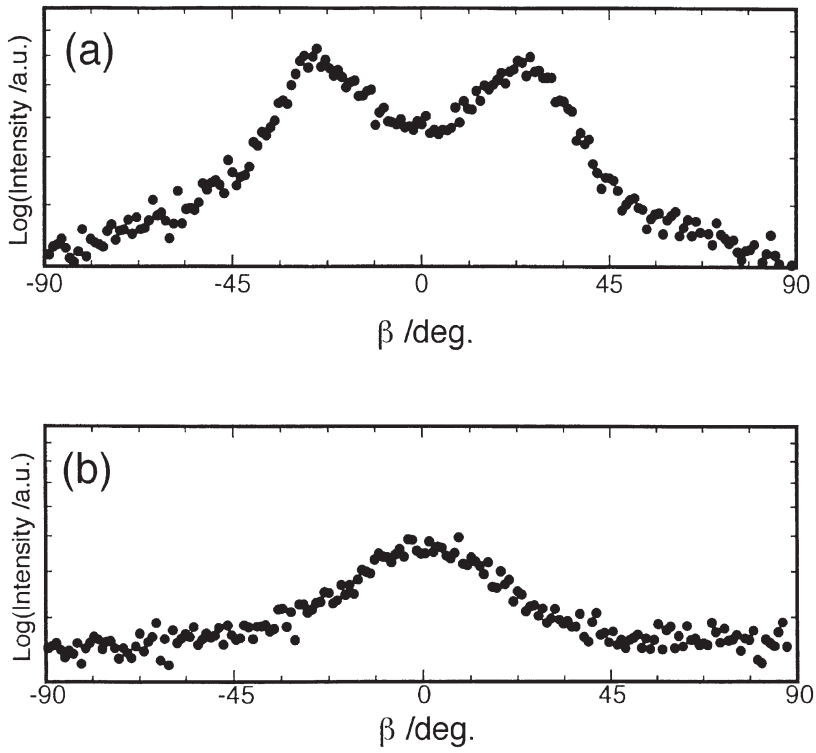

Figure 13. Intensity distribution $I(\beta)$ measured as a function of the azimuthal angle β at a diffraction angle of $2\theta = 20.5^\circ$. Curves (a) and (b) are collected from Figure 12(a) and 12(b), respectively. The equatorial direction corresponds to $\beta = 0^\circ$.

taken from three characteristic positions to the film. In the X-ray pattern of Figure 12(a), taken with the beam irradiation parallel to the film surface and perpendicular to the oriented axis (chain axis), layer reflections appear on the meridian and broad reflections are split above and below the equator. The splitting of the broad reflections can be seen more clearly in curve (a) of Figure 13 where the intensity distribution $I(\beta)$ was measured as a function of the azimuthal angle β at a constant diffraction angle of the reflection ($2\theta = 20.5^\circ$). In contrast, when the X-ray beam is irradiated perpendicular to the film surface, the layer reflections are invariably observed on the meridian, but the broad reflections are concentrated on the equator (see Figure 12(b) and curve (b) of Figure 13). On X-ray irradiation parallel to both the film surface and the chain axis, only broad reflections can be observed without any orientation (Figure 12(c)). These diffraction profiles dictate the biaxiallity of the S_{CA} phase, in which the zigzag tilting of mesogenic groups takes place in a direction perpendicular to the film surface, as illustrated in Figure 14(a).

DESIGN OF FERROELECTRIC SMECTIC PHASES IN ACHIRAL SYSTEM

In addition to the conformational constraint, another interesting effect can be considered on the smectic structure of main-chain LC polymer when the two different alkyl spacers are introduced in a regularly alternate fashion (refer to Figure 15).[32] If the two spacers are incompatible, or if there is a sufficient lateral attraction between identical spacers of adjacent polymer molecules, segregation into the bilayer may occur. Then, four possible types of bilayer structures will arise as a result of a coupling with conformational constraint mentioned above. These are illustrated in Figures 16a–16d. The bilayer structures of Figures 16a and 16b may be formed from the polymers in which both different spacers have even number of carbons. The bilayer smectic phase in Figure 16c may arise in the polymers with the two spacers different in an odd-even parity of their carbon number. Finally, the bilayer phase of Figure 16d can be expected for the polymers in which both spacers have the odd carbon number.

The bilayer smectic phase of Figure 16d is especially interesting since it should be ferroelectric even in non-chiral system. Its ferroelectricity can be understood by considering the space group. As illustrated in Figure 17, the space group is analogous to the crystallographic C_{2v}; there are two fold axes along y-axis and mirror planes perpendicular to x- and z-axes.[33] Since there is no mirror plane perpendicular to the two fold axes, the spontaneous polarization can be expected to arise along the y-axis, *i.e.*, in a tilted direction of molecule in a layer.

This type of ferroelectric smectic liquid crystal has

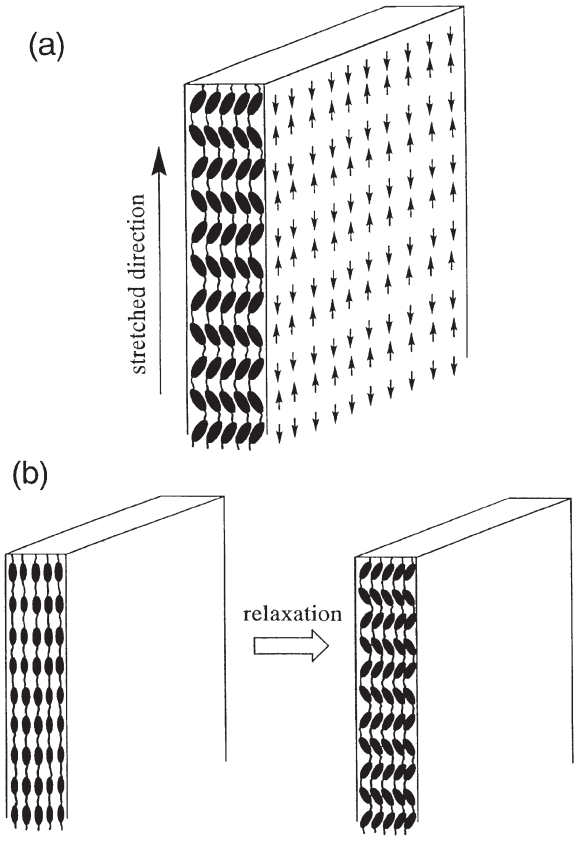

Figure 14. (a) Illustration of biaxial orientation of zigzag molecules in the S_{CA} film where the mesogenic groups are tilted in a direction perpendicular to the film surface. This preferential orientation may be caused by relaxation from the extended arrangement of mesogenic groups on drawing to the stable zigzag arrangement illustrated in (b).

been sought in the following main-chain LC polymers with two odd-numbered aliphatic chains sequenced in a regularly alternate fashion.[11]

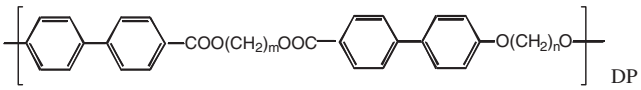

Here, the aliphatic chain containing three methylene units is connected to the mesogenic cores by ester linkage groups, while the other aliphatic chain with odd n (= 3–15) is linked to the mesogenic cores by ether linkage groups. The polymers were designated BP-CO3-O*n* where 3 and *n* indicate the numbers of methylene groups in the spacers. All the polymers form the smectic phases.

Smectic Layer Structure as Elucidated from X-ray Pattern

Depending on the compatibility of two flexible spacers, two possible types of smectic structures can be considered to be formed. One is a single-layer smectic phase in which the two different spacers are compatible and so randomly mixed. Another is a bilayer smectic phase with the different spacers segregated from each other. These two types of layer struc-

Figure 15. Illustration of main-chain LC polymer with two different spacers sequenced in a regularly alternate fashion.

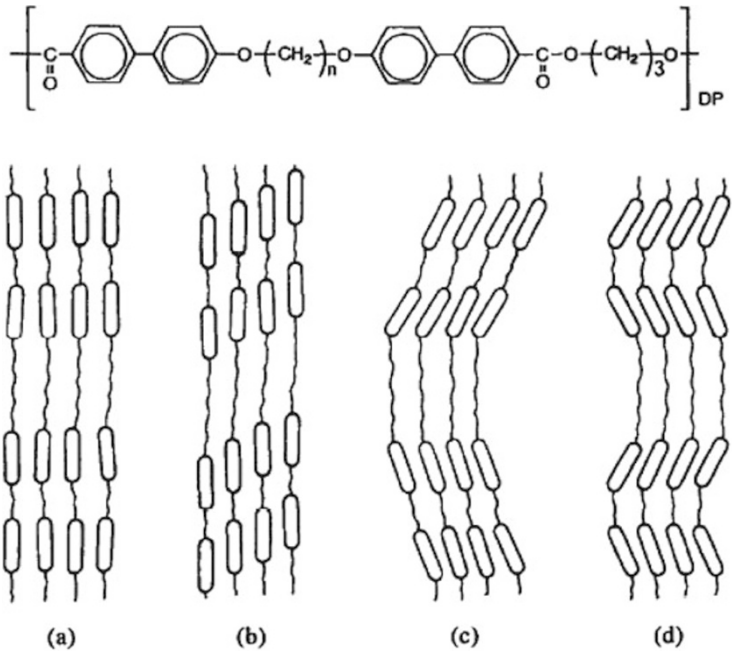

Figure 16. Four possible smectic structures with the bilayer modifications which may be formed in the main-chain LC polymers of Figure 15.

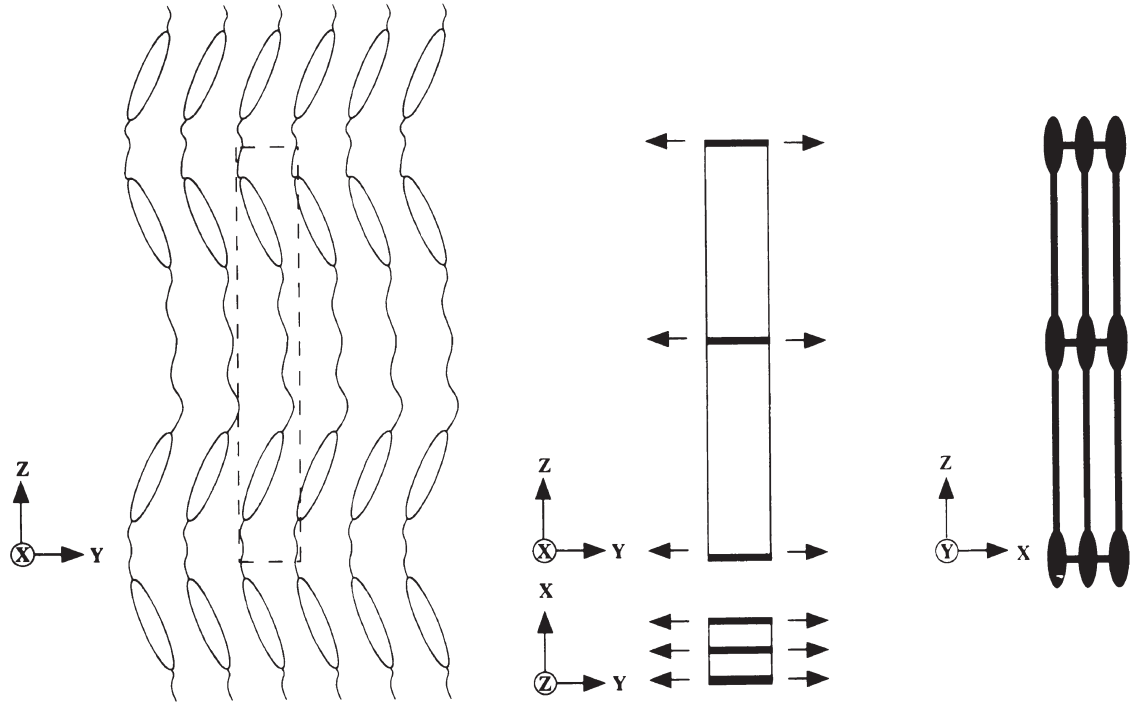

Figure 17. Space-group symmetry for the bilayer smectic structure of Figure 16d.

tures can be easily distinguished from each other through X-ray observations. In random mixing system, the first-order layer reflection should possess a spacing corresponding to half a length of repeat unit ($L/2$) while in the bilayer system it arises with a spacing corresponding to the length of repeat unit (L).

Figure 18a shows the X-ray diffraction pattern observed for the oriented smectic phase of BP-CO3-O7. A similar X-ray pattern is observed for BP-CO3-O3, BP-CO3-O5 and BP-CO3-O9. For these polymers with $n = 3$ to 9, the first-order layer reflections (the 001 reflections) appear with the spacings of 12.9 Å to 16.1 Å as listed in Table I. These values approximate half a repeat length ($L/2$), meaning that the layer structure is constructed by a random mixing of the two different spacers. The type of smectic phase is S_{CA}, as clarified from diffraction geometry in Figure 18a.

The remarkably distinct X-ray pattern is observed for the smectic phases of BP-CO3-O11, BP-CO3-O13 and BP-CO3-O15 with larger n, as shown in Figure 18b. An interesting aspect of this pattern is that the meridional layer reflection is accompanied by four point (off-meridional) reflections (see enlarged photograph in Figure 18b). As listed in Table I, the spacing of the first meridional reflection corresponds to half a length of repeat unit ($L/2$) while the off-meridional reflections appear with the height of $1/L$ far from the equator. This shows that there is a density modulation with a periodicity of L along the layer normal. The X-ray photograph shows additionally weak but distinct higher order reflections on meridian and off-meridian, which are also listed in Table I. All of these

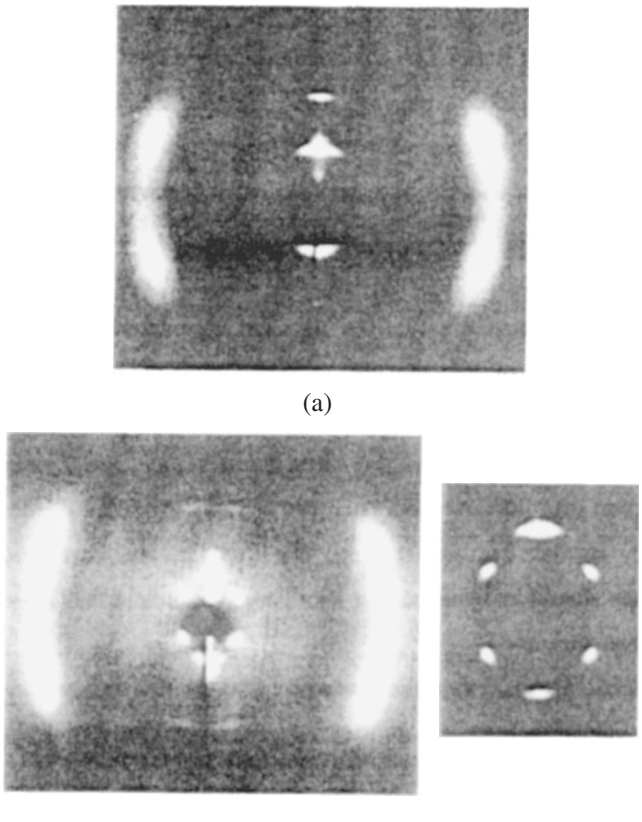

(a)

(b)

Figure 18. X-ray diffraction photographs of the oriented smectic phase observed in (a) BP-CO3-O7 and (b) BP-CO3-O11 fibers at 200 °C. The fiber specimen was prepared by pulling up the isotropic melt and its axis is placed in the vertical direction. The enlarged photograph in (b) shows the X-ray pattern in a small-angle region.

Table I. Spacing (Å) of layer reflections for smectic phases of BP-CO3-O*n* polymers*

BP-CO3-O3	BP-CO3-O5	BP-CO3-O7	BP-CO3-O9	BP-CO3-O11	BP-CO3-O13	BP-CO3-15
				21.9 (101)	24.7 (101)	26.5 (101)
12.9 (001)	13.9 (001)	14.9 (001)	16.1 (001)	17.1 (002)	18.0 (002)	19.0 (002)
						12.1 (103)
6.43 (002)	6.94 (002)	7.45 (002)		8.54 (004)	9.04 (004)	9.51 (004)
				6.66 (105)		
				5.70 (006)	6.02 (006)	6.34 (006)

*Figures in parentheses are indices of reflections (see text).

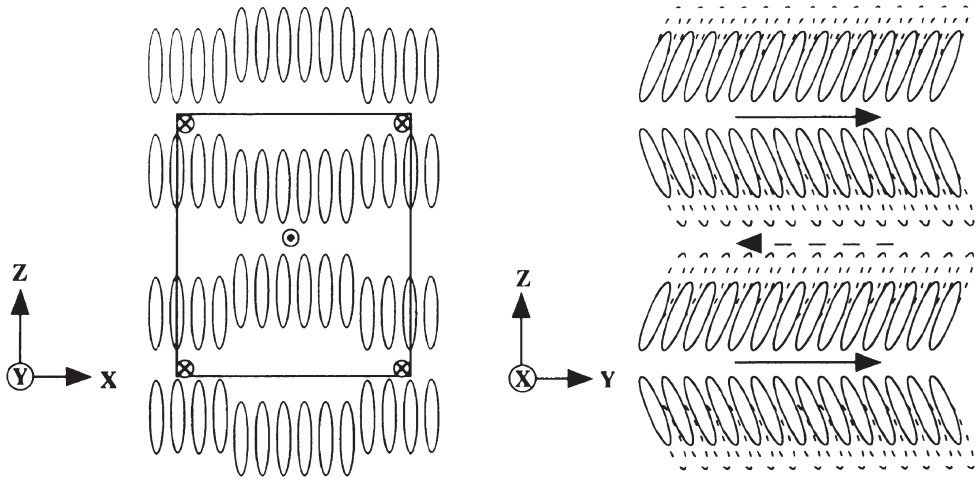

Figure 19. Tentative structural model for the frustrated smectic phase.

reflections can be interpreted as $00l$ ($l = 2m$) and $10l$ ($l = 2m + 1$) reflections based on the two-dimensional rectangular lattice. The lattice parameters are determined as $a = 28.5$ Å and $c = 34.2$ Å for BP-CO3-O11, $a = 33.8$ Å and $c = 36.2$ Å for BP-CO3-O13 and $a = 38.9$ Å and $c = 37.8$ Å for BP-CO3-O15. Here, the *c*-axis corresponds to the polymer chain axis and *a*-axis lies perpendicular to the polymer chain. Considering that the averaged diameter of molecule is more or less than 4.5 Å, six to eight molecules are located in these lattices. Diffuse outer reflections are also observed here, lying above and below the equator. Hence, the mesogenic groups are liquid-like in a layer and their axes are alternately tilted to the layer normal similarly as in the S_{CA} phase of the random mixing system. Overall results show that the smectic phase forms the bilayer structure of Figure 16d although it also has another periodic density modulation in a direction parallel to the layer irrespective of the liquid-like lateral association of mesogenic groups.

Layer Structure Responsible for Distinct X-ray Pattern Showing Meridional and Off-Meridional Layer Reflections

The characteristic pattern of Figure 18b containing the meridional and off-meridional layer reflections is reminiscent for the frustrated smectic phases,[4–36] and a structural model is proposed as illustrated in Figure 19. Here, the internal structure of the smectic layers displays an unusual density modulation perpendicular to the tilt direction of mesogenic groups.[37] The unusual density modulation can be produced in such a way that the bilayer is constructed by a repeat unit of polymer chain in a small domain but the polymer chains in adjacent domain slide halfway along the layer normal after the 180° rotation around their chain axes. In other words, this density modulation can be described by a periodic structure of domain walls, in each domain the basic layer structure being the same as the bilayer structure of Figure 16d. Observation of a series of reflections with $l = 1$ to 5 dictates the highly positional order along the layer normal (c-axis) while the positional order along the layer (a-axis) is low because of the observation of reflections with only $h = 1$. This shows that the density modulation along the layer is not necessarily regular. Furthermore, tilted orientation correlation of the mesogenic groups, which should be required in a liquid crystalline field, is maintained irrespective of the frustration.

The frustrated smectic phases with a two-dimensionally positional order were first observed for low molar mass compounds such as the derivatives of cyanobiphenyl possessing a strong longitudinal dipole.[34] Frustration effects arise in such a system because of the incommensurability of two types of characteristic

Table II. Characterization of BB-*n* polyesters

		Calorimetric Data					
		Transition temperatures				Transition enthalpies	
		Heating		Cooling			
Sample	η_{inh}/dL g^{-1}	T_m/°C	T_i/°C	T_c/°C	T_i/°C	ΔH_c/kJ mol^{-1}	ΔH_i/kJ mol^{-1}
BB-6-I	0.26	210	231	187	218	13.05	8.33
BB-6-II	0.34	213	238	167	228	8.74	9.67
BB-6-III	0.40	216	239	166	227	8.74	8.24
BB-6-IV	0.49	214	240	165	229	7.94	8.41
BB-6-V	0.67	220	241	161	227	7.69	8.91
BB-6-VI	0.92	210	239	155	224	8.20	10.46
BB-8	0.70	193		153	180	6.78	9.50
BB-10	0.84	171		151		16.23	
BB-12	1.05	164		141		19.71	

[a]Based on DSC data measured at a scanning rate of 10 °C min^{-1}.

lengths, namely, the molecular length and the pair length, the pair formation being controlled by dipolar forces. In the present system, can one make sense for the driving force for the adoption of such a frustrated smectic phase? If the fundamental bilayer smectic phase of Figure 16d is ferroelectric, it turns out that the answer is rather simple. By comparison with the ferroelectric bilayer of Figure 16d, there is a two dimensional escape of polarization, *i.e.*, an antiferroelectric arrangement of polarization in the frustrated smectic phase of Figure 19. It is thus postulated that the frustration is induced to eliminate the strong interaction of the spontaneous polarization.

According to the same argument on the packing symmetry, more recently, ferroelectric and antiferroelectric liquid crystals in achiral system have been discovered on the low molecular weight materials, twin dimers and banana molecules, by our group.[38–40] Typical banana molecule is given below.

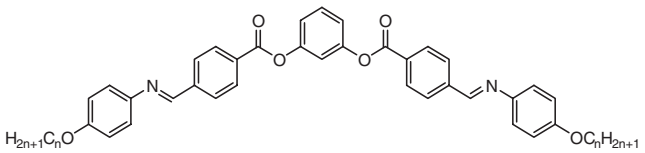

In these nonchiral molecular systems, it is interesting that there is a simultaneous formation of chiral structure.[41–45] The polarity and chirality as well as frustration have become a world wide topics in the liquid crystalline field.[46] It should be emphasized that studies on these exotic phases start from the studies on the polymeric effects in main-chain LC polymers.

CHAIN FOLDING IN SMECTIC PHASE

The preceding sections show that the polymer takes up the relatively extended configuration at least in a local space of smectic liquid crystal field. However, it has not been clarified whether the polymer chains are extended along the entire length or not.

This important structural aspect on polymer chain configuration in a liquid crystal field has been extensively debated theoretically.[47–49] The complexity and subtlety in the main-chain LC polymers come from the interplay between long-range orientational order of the liquid crystals and the polymeric tendency to maximize entropy. de Gennes[47] first pointed out that a semiflexible polymer chain in nematic phase may recover some part of the entropy loss due to the ordering of mesogenic units by forming hairpin foldings where the chain executes a counter reversal (180°) with respect to the n-director. The existence of one or two hairpin foldings has been established by small-angle neutron scattering measurement in the nematic phase of main-chain polymers.[50–53] This section represents the solid state morphology of BB-6 by small-angle X-ray scattering (SAXS) method and discusses the chain configuration in the smectic phase.[16–19]

Chain Folding Lamellar Structure in BB-6 Crystal Formed from S_A Melt

Six specimens with different molecular weights, BB-6-I to BB-6-VI, were prepared. All the polymers exhibit the well-defined transition behavior as listed in Table II. The two transitions at T_m and T_i can be assigned to the crystal melting to S_A phase and the isotropization of S_A phase, respectively.

Parts a and b of Figure 20 show the wide-angle X-ray diffraction pattern and SAXS pattern for the crystalline BB-6 specimen, respectively. Here, the sample was prepared by crystallizing the smectic melt which was sheared and oriented. For crystallized sample, the orientational order of the smectic phase is completely sustained, and as found in Figure 20b, clear reflection

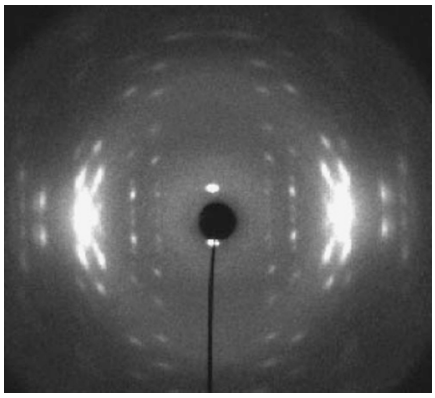

(a)

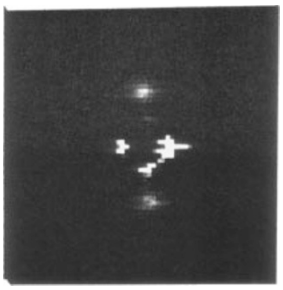

(b)

Figure 20. (a) Wide-ange and (b) small-angle X-ray patterns of the crystalline phase of BB-6-III. Here, the oriented film specimen was prepared by shear flowing the smectic A phase between glass plates. The flow direction is horizontal.

maxima with spacing around 250 Å can be seen on the meridian, showing the long period along the chain axis. Takahashi and Nagata[54] reported an electron microscopic observation for the same BB-6 crystal sample and concluded the formation of the characteristic stacked lamellar structure in which the 250 Å thick lamellae are superimposed on smectic-fan texture. The thickness of lamellae corresponds to the long period observed in our work.

The lamellar spacings by SAXS were determined for all the polymers and are listed in Table III. To prevent thermal prehistory, the data were collected for the crystals cooled at a rate of $10\,^{\circ}\mathrm{C\,min^{-1}}$ after 5 min of annealing in the isotropic melt. The lamella spacing, L, is distributed around 250 Å, increasing somewhat with an increase of molecular weight. This trend is reasonably explained in the next part of this section. The correlation length between foldings thus corresponds to approximately 15 times the length of the repeat unit. The values for the average number of foldings in a chain, F, are listed in Table III as calculated from the equation, $F = l/L - 1$ where l is the whole length of polymer. It is found that several foldings are included in a chain.

Here it should be recalled that the crystallization of the BB-6 polymer takes place from the S_A melt, but not from the isotropic melt. The S_A phase has a long range orientational order and one-dimensional positional order. If the polymer chain is extended along its entire length in the S_A phase, it must fold at the crystallization with falling out of the order of the smectic liquid crystal. In practice, however, not only the orientational order of the smectic phase (see Figure 20a), but also characteristic smectic-like texture and defects[54] are completely sustained on crystallization. We therefore conclude that the chain folding observed in the crystalline phase already exists in the preceding S_A phase.

Anomalous Dependence of Lamellar Spacing on Crystallization Temperature

SAXS measurements were performed for the crystalline BB-*n* specimens with various crystallization temperatures (T_c). Here, four BB-*n* polyesters, namely, BB-6, BB-8, BB-10 and BB-12 were used. As listed in Table II, BB-6 and BB-8 form isotropic liquid, S_A and crystalline phases in order of decreasing temperature, thus they crystallize from S_A mesophase. On the other hand, BB-10 and BB-12 with longer spacer crystallize from the isotropic liquid as conventional polymers. It is interesting to compare the crystallization behavior of these two homologues.

To secure a wide range of T_c and prevent effects of annealing at high temperature, the samples were prepared by cooling from the preceding phase (the S_A

Table III. Parameters for the lamellar structure formed by folded chains of BB-6

Sample	M_n	M_w/M_n	Chain length l^a/Å	Lamellar size L^b/Å	Number of chain folding F^c
BB-6-I	1.28×10^4	2.41	7.8×10^2	225	2.5
BB-6-II	1.36×10^4	2.39	8.3×10^2	244	2.4
BB-6-III	1.52×10^4	2.03	9.2×10^2	251	2.7
BB-6-IV	1.70×10^4	2.46	1.0×10^3	247	3.2
BB-6-V	2.15×10^4	2.38	1.3×10^3	267	3.9
BB-6-VI	3.23×10^4	2.30	2.0×10^3	294	5.5

[a]Calculated using repeating length of 19.6 Å in the crystalline state. [b]Observed for the crystal sample cooled from the isotropic melt at a rate of $10\,^{\circ}\mathrm{C\,min^{-1}}$. [c]$F = l/L - 1$.

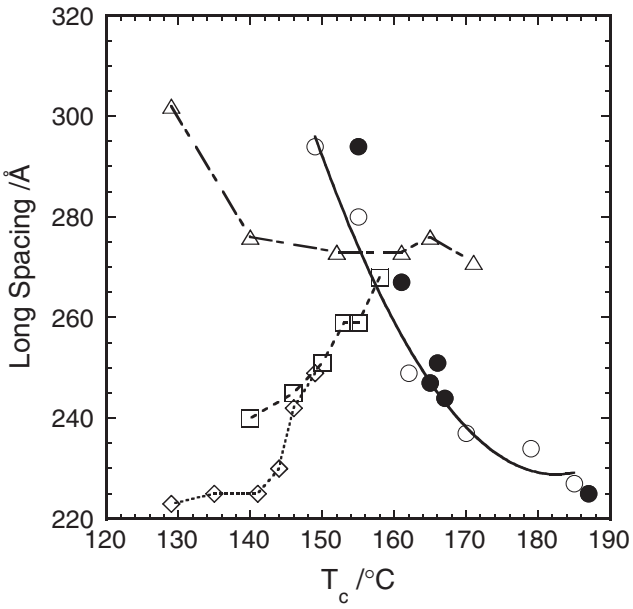

Figure 21. Plots of lamellar spacing of BB-6 (circle), BB-8 (triangle), BB-10 (square) and BB-12 (lozenge) crystals as crystallized from the preceding phase (the S_A phase in BB-6 and BB-8 and the isotropic melt in BB-10 and BB-12) against the crystallization temperature. Here, the open symbols were collected from the samples prepared by cooling at different cooling rates and the closed circles were obtained from the BB-6 samples with different molecular weights which were cooled at a rate of $10\,^{\circ}\mathrm{C\,min^{-1}}$ (refer to Tables II and III).

phase for BB-6 and BB-8 and the isotropic phase for BB-10 and BB-12) at various rates (1.25 to 40 $^{\circ}\mathrm{C\,min^{-1}}$). Figure 21 shows the dependence of the lamellar spacing (L) on the T_c. Opposite trends are found between the specimens crystallized from the isotropic liquid (BB-10 and BB-12) and those crystallized from the S_A phase (BB-6 and BB-8). In the former, the lamellar spacing increases with an increase in T_c, which can be understood from the kinetical criteria as considered in conventional polymers.[56] In the latter, in contrast, it decreases with an increase in T_c.

Here, the effect of molecular weight on the lamellar spacing for BB-6 is reconsidered (see Table III). The lamellar spacings were determined for samples with different molecular weights (BB-6-I $\sim$ BB-6-VI) cooled from S_A phase to room temperature at a constant rate of $10\,^{\circ}\mathrm{C\,min^{-1}}$. T_c decreases with an increase in molecular weight. The data are plotted in Figure 21 with closed circles, showing the identical relationship with the data (open circles) collected for one sample (BB-6-IV) cooled at various rates. It is thus reasonable to assert that the lamellar spacing depends on the crystallization temperature rather than the molecular weight.

Chain Folding in Smectic Phase

The unusual dependence of the lamellar size on T_c in BB-6 and BB-8 crystals suggests that the chain foldings result from a completely different origin from conventional polymers, and it can be interpreted based on an assumption that the chain folding has already existed in the preceding S_A mesophase. In the fluid liquid crystalline field, the hairpin fold may be reasonably occur to recover some part of entropy loss due to the ordering of the mesogenic units and its probability increases with the increase of temperature. In other words, the fold length decreases with increasing temperature, showing that the lamellar thickness in the resulting crystal decreases with increasing crystallization temperature.

The quantitative argument on the temperature dependence of the chain folding length has been done by Warner and coworkers.[48,49] They have developed statics and dynamics of chain foldings in worm-like chains and given the simple theory in which the fold length is proportional to $\exp(U_h/k_BT)$ where $U_h = 2\sqrt{3aS\varepsilon}$ is the hairpin energy, S, the order parameter of the LC field, ε, the elastic bend constant, and a, the LC field coupling constant. To clarify this proportionality, the logarithmic lamellar spacings are plotted against the reciprocal of absolute temperature in Figure 22 for BB-6 and BB-8. A linear relationship between the two can be seen as expected from the above equation. Here, it is reasonable that the slope of the line of BB-6 is larger than that of BB-8 since it reflects the chain rigidity estimated by ε. The hairpin theory for the preceding LC phase thus explicates the variation of lamellar size in BB-6 and BB-8 crystals, showing that the chain folding exists at thermodynamic equilibrium as an entropy effect in the preceding S_A phase.

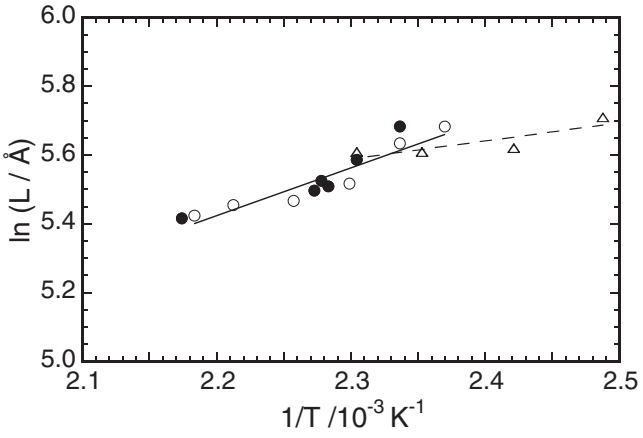

Figure 22. Plots of logarithmic lamellar spacing against the reciprocal of the crystallization temperature (T_c) for BB-6-IV (circles) and BB-8 (triangles). The data points given by the open symbols are those observed in Figure 21. Also included are the data points given by closed symbols collected for the BB-6 polyesters with different molecular weights.

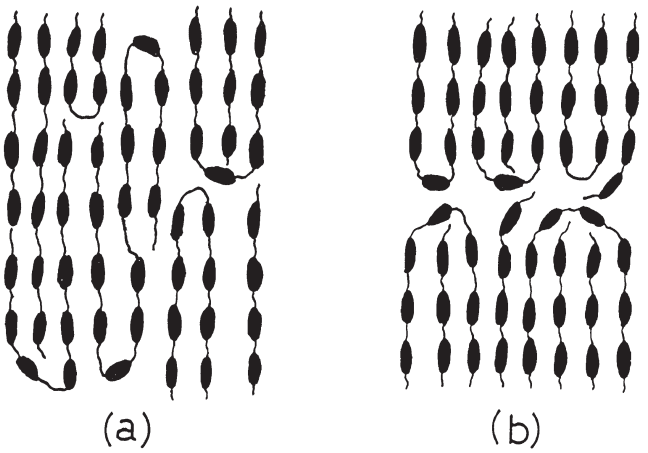

Figure 23. Two possible schematic diagrams showing the different accommodation of the chain folding sites into the smectic structure. In (a), the folding sites are randomly placed, while in (b), segregated to form domain boundaries.

Unusual Orientation of Smectic Melt on Uniaxial Stretching and Shear Flow That Is Explained by Chain Folded Lamellar Structure

The question arises as to how the chain folding is accommodated in the S_A or S_{CA} phase. Two possible schematic diagrams are shown in Figure 23. In one model, the chain foldings are positioned randomly (Figure 23a), and in another they are segregated at a certain confined position to result in the lamellar type of domain boundaries like in the crystalline phase (Figure 23b).

Regarding this aspect, an anomalous molecular orientation in the fibers drawn from the smectic melts is interesting.[1,12,18,19,57–60] Figure 24b shows X-ray pattern taken for such a fiber of BB-5. The pattern is similar to that (Figure 24a) of the fiber drawn from the isotropic melt, but quite different in the orientation geometry of reflections with respect to the fiber axis. The layer reflections in smectic melt-spun fibers appear on the equator, showing that the smectic layers lie parallel to the fiber axis, *i.e.*, the polymer chain axis orients perpendicular to the elongation direction. Such a type of flow has been observed in low molecular weight smectic phases and can be easily understood since each smectic layer is composed of the molecules (refer to Figure 25a) and flow takes place by mutual slip of layers. In the polymeric system, however, this mechanism is not acceptable since the mesogenic groups in neighboring layers are linked to each other through a flexible spacer and so each polymer molecule passes through many smectic layers. To explain this unusual orientation, we postulate that the chain-folded lamellar domains form in the smectic field and their flow takes place between lamellae (see Figure 25b).

Decisive evidence for existence of the chain folded

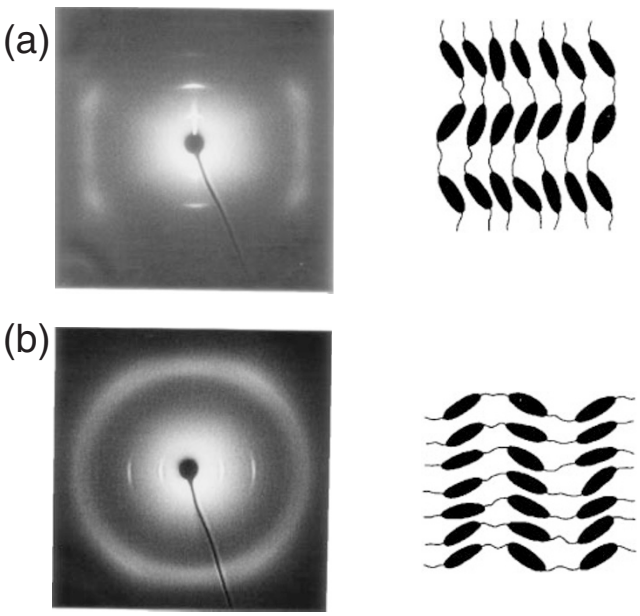

Figure 24. X-ray photographs for (a) fiber A drawn from the isotropic melt of BB-5 at a rate of around 1 m sec^{-1} and (b) fiber B drawn from the smectic melt of BB-5 at a rate of 1 cm sec^{-1}. The fiber axis is in the vertical direction. The molecular arrangements deduced from the X-ray patterns are also illustrated.

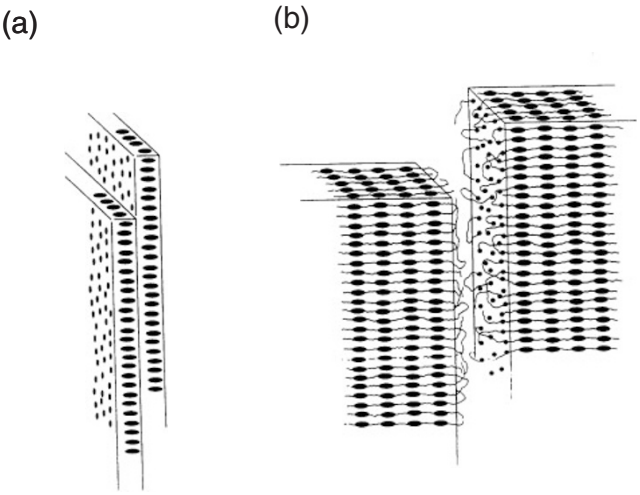

Figure 25. Schematic comparison of the flow of (a) the low molecular mass smectic phase and (b) polymeric smectic phase. In the polymeric system, lamellae are formed and slip over each other while in the low molecular mass system, smectic layers slip over each other.

lamellae in the smectic liquid crystal has been obtained from the studies on shear-flow orientation of S_{CA} melt of following BB-5(3-Me).

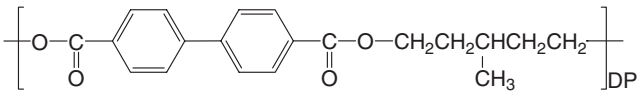

Two types of orientation can be observed mainly depending on temperature. By shear flow at tempera-

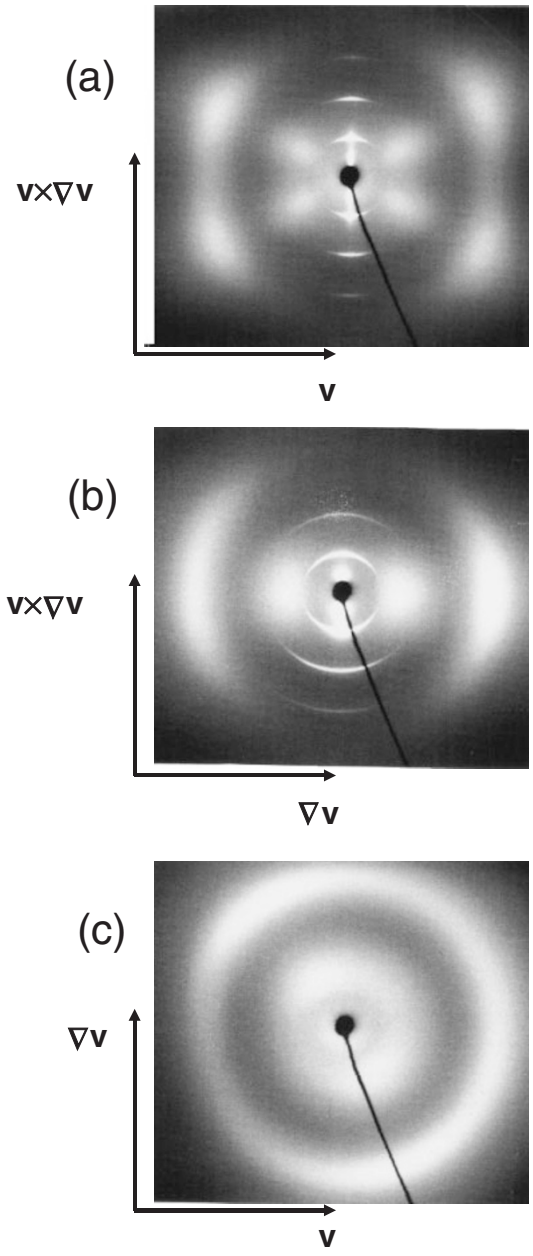

Figure 26. Wide-angle X-ray diffraction patterns for the BB-5(3-Me) sheared at a rate of $0.214\,s^{-1}$ at 140 °C. These patterns indicate a perpendicular layer orientation. The broad inner hallows with the spacing of around 8 Å appearing in (a)–(c) are scattering due to continuous X-rays remaining in Ni-filtered X-ray. The intensity inequality in the outer broad halo in (c) was inconsistent throughout the measurements.

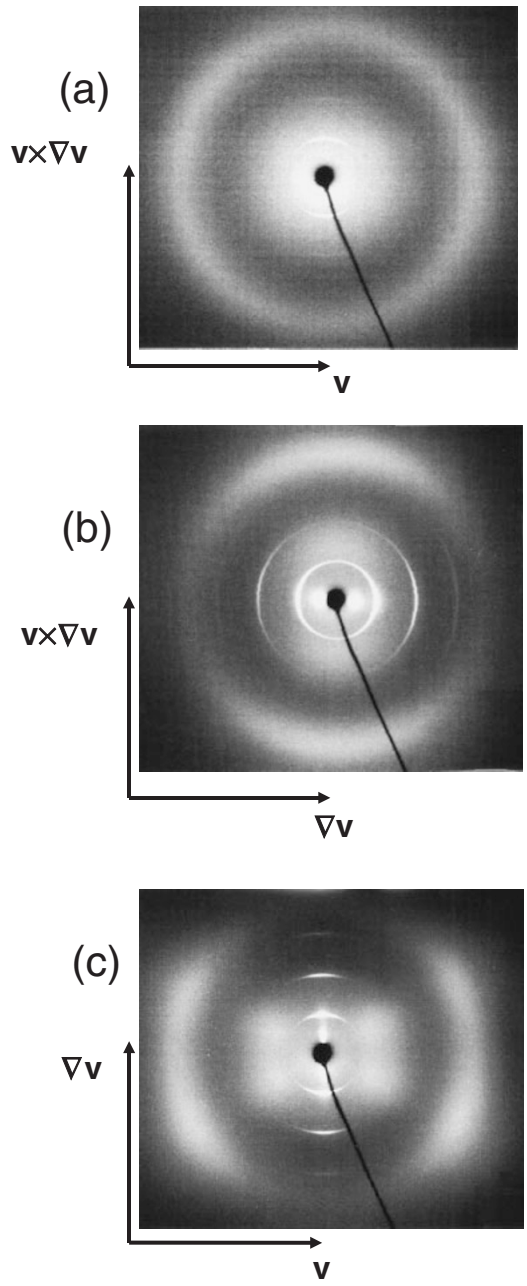

Figure 27. Wide-angle X-ray diffraction patterns for the BB-5(3-Me) sheared at a rate of $6.38 \times 10^{-3}\,s^{-1}$ at 130 °C. These patterns indicate parallel layer orientation. The broad inner hallows with the spacing of around 8 Å in (b) and (c) are scattering due to continuous X-rays remaining in Ni-filtered X-ray.

tures close to the isotropization temperature (T_i), the S_{CA} phase is oriented with the layer normal parallel to the vorticity direction (so-called "perpendicular orientation") as shown in Figures 26 and 28a, whereas it is oriented with the layer normal parallel to the velocity gradient direction ("parallel orientation") as shown in Figures 27 and 28b by shear flow at temperatures enough below T_i. The orientation mechanism of these two types is explained as follows.

The S_{CA} phase is the fluid smectic phase where the mesogen centers of mass have a one-dimensional layer order along the n-director, but are isotropically distributed within a smectic layer. If the shear flow occurs based on the intrinsic fluidity of molecules, the smectic phase would not show the transverse orientation with the polymer chains lying parallel to the shear direction as typically observed in the nematic liquid crystal. In place of the transverse orientation, it exhibits perpendicular orientation since the molecules can flow only within a layer, *i.e.*, maintaining the layer or-

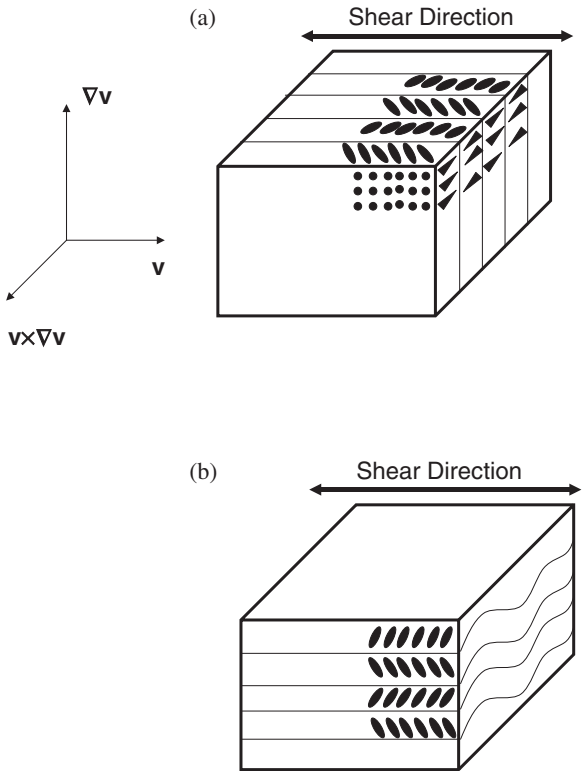

Figure 28. Illustration of perpendicular (a) and parallel (b) orientations in the shear oriented S_{CA} specimen. In (a), the arrows depicted in the side of the rectangular parallelepiped mean that the mesogens are tilted respect to the layer normal in the shear plane as seen in the upper face. In (b), the wave lines in the side of the rectangular parallelepiped indicate that the smectic layers undulate along the vorticity direction.

dering. Parallel orientation cannot be achieved at all by the intrinsic fluidity of molecules, but by the mutual slip of smectic layers. However, such a slip is impossible in the polymeric system since the polymer chain passes through many smectic layers as mentioned above. The slipping unit should be a chain folded lamella.

The chain folded lamella in the parallel orientation has been detected with synchrotron radiation small-angle X-ray scattering method (Figure 29). The long period is about 80 Å which is five times as long as the repeat unit length of BB-5(3-Me) (16.4 Å). This lamella spacing is much smaller than those of around 250 Å proposed for the S_A phase in the previous part of this section,[16,17,19] suggesting that shear flow in the smectic liquid crystal may affect the lamellar thickness. Here, it should be stated that the spacing of 80 Å is comparable to the value estimated by a theoretical treatment of the effects of shear flow on the parallel oriented lamellae at microscopic level where the lamellar spacing (d) is connected with the critical stress for the layer collapse (disorientation) ($(\eta\dot{\gamma})_c$) and the lamellar binding energy (K) as[61,62]

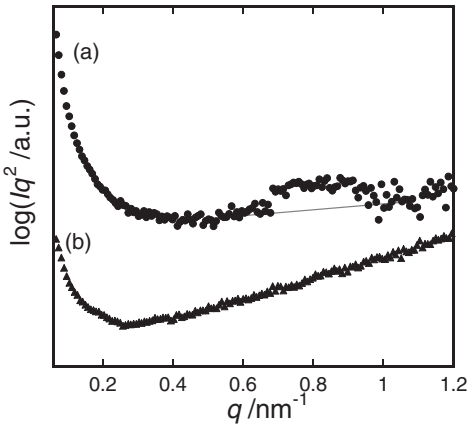

Figure 29. SR-SAXS profile of the parallel oriented BB-5(3-Me) (a) in the velocity gradient direction and (b) in the shear flow direction recorded by irradiating X-ray beam in the vorticity direction. The specimen was prepared by shearing the smectic melt at $6.38 \times 10^{-3}\,s^{-1}$ at 130 °C.

$$(\eta\dot{\gamma})_c \cong \frac{(k_B T)^{5/2}}{K^{3/2} d^3}. \qquad (1)$$

Here we assume that $K \sim k_B T_i$ (T_i is the isotropization temperature of BB-5(3-Me), 423 K) and that $(\eta\dot{\gamma})_c$ equals the maximum stress of 3.0×10^3 Pa appearing on shearing the parallel oriented sample to transform to the perpendicular oriented one at 140 °C, and obtain $d \sim 120$ Å. The calculated lamellar spacing of 120 Å is comparable to the lamellar spacing of 80 Å rather than the smectic layer spacing of 16.4 Å. Thus, the parallel orientation of the polymer smectic liquid crystal is reasonably attributed to the mutual slide of the chain folded lamellae.

As shown in Figure 30, the type of the orientation depends on temperature and shear rate. At higher temperatures, the perpendicular orientation is preferred, while at lower temperatures the parallel orientation is observed. This clear temperature dependence can be connected to temperature dependence of the friction of the mesogens within the layer. The packing of mesogens within a layer is more liquid-like at higher smectic temperatures, allowing the molecules to fluid within a layer. However, it may become solid-like at lower temperatures. As a result, the shear gradient prefers the mutual slide of the chain-folded lamellae whose boundary may possess more fluidity to the internal flow with hard friction of mesogens within a smectic layer.[22]

Hairpin Folding in Nematic Liquid Crystalline Field

The hairpin folding may significant in the nematic liquid crystal, which has the least order and the highest symmetry. The molecules are mobile in three dimensional directions.[63] Thus, the formation and elimination of the chain folds in the nematic field

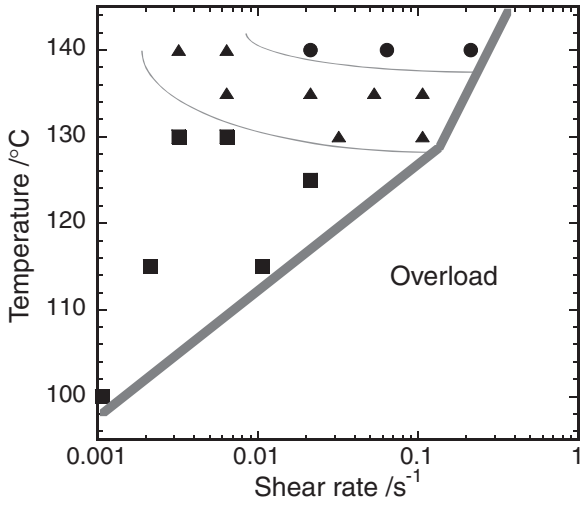

Figure 30. Shear rate – temperature diagram in smectic layer orientation for the S_{CA} mesophase of the BB-5(3-Me) subjected to steady shearing. Circle and square symbols refer to perpendicular, parallel orientations, respectively. Triangle symbols indicate the intermediate orientation in which both the parallel and perpendicular orientations coexist. The shear rates and the temperatures in the lower right hand region in the figure were not determined because the apparent torque was over the mechanical range of the rheometer.

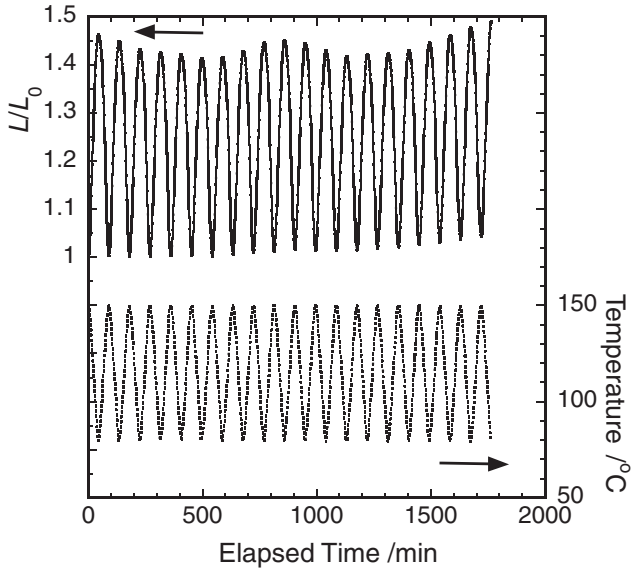

Figure 31. Repeatability of change of the relative length (L/L_0) of the oriented nematic elastomer by heating and cooling cycles between 150 and 80 °C at a rate of 2 °C min^{-1}.

would reflect on the sample length along the director. This has been examined in a monodomain nematic elastomer.[64]

Figure 31 shows the change of sample length along the nematic director by heating and cooling cycles in the nematic temperature range between 80 °C and 150 °C. Here, L_0 is the sample length at 150 °C determined at the beginning of the measurement and the relative length L/L_0 and the temperature are plotted against time. The elastomer is expanded along the nematic director (polymer chain direction) on cooling and contracted reversibly on heating in the nematic LC state. The degree of expansion or contraction was about 45% in the temperature range of 80 to 150 °C. The shape change took place with a constant orientational order. This characteristic thermoelastic behavior is explainable if the polymer chain connecting the cross-link points includes several hairpins, the probability of which is proportional to the Boltzmann factor of hairpin energy. The hairpin energy deduced from the temperature dependence of the length of nematic elastomer was 3.8×10^{-20} J, which are comparable to those estimated from the SANS data for other nematic main-chain polyesters.[50–53]

SMECTIC LIQUID CRYSTALLINE GLASS

Typical thermotropic LC materials form isotropic liquid, LC and crystal phases in an order of decreasing temperature. However, some LC materials solidify without crystallization. The resulting solid is hence regarded as liquid crystal glass.[18,23,24,65–78] While conventional glass, namely isotropic liquid glass, is characterized by an absence of long-range order, the nematic LC glass possesses a simple orientational order of rod-like molecules and the smectic LC glass has the long-range one-dimensional positional order as well. These LC glasses are thus expected to provide new insight into dynamics of glassy materials representing a topic of current interest in condensed matter physics.

Representative Smectic LC Glass Prepared from BB-5 and its Thermal and Mechanical Properties

In the liquid state, a polymer molecule is capable of assuming a large number of conformations due to the rotational freedom of individual chain atom about their connecting bonds. There is no significant correlation between conformations assumed by the individual molecules so that the liquid state is characterized with random, haphazard arrangements of the polymer chain segments. In the LC phase, a long range orientational order requires polymers to take some extended conformations. Starting from coiled, mutually interpenetrating macromolecules, these specified conformations in the LC phase seem hardly to be achieved instantaneously from purely kinetic reasons. We thus have a significant question as to whether the isotropic phase can be transformed to the LC phase completely or not in the LC polymeric system.

To examine this point, the isotropization enthalpy, ΔH_i, was measured for the S_{CA} phase of BB-5 formed under an isothermal condition. On this measurement, BB-5 polyester was quenched to the S_{CA} phase of

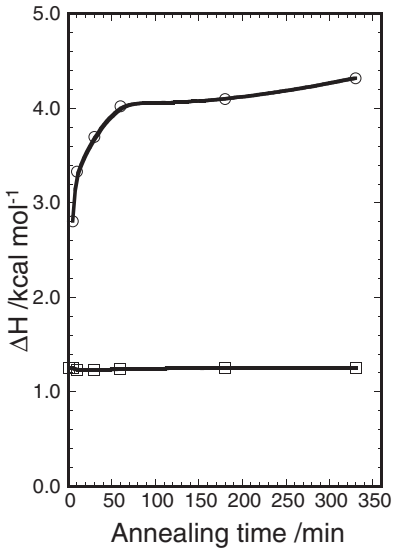

Figure 32. Variation in isotropization enthalpy, ΔH_i (rectangles), and crystal melting enthalpy, ΔH_m (circles), for BB-5 with the isothermal formation time. ΔH_i (or ΔH_m) was measured for the sample which was quenched from the isotropic (or S_{CA}) phase and held at 185 °C (or at 140 °C) during a certain period for isothermal formation of the S_{CA} (or crystal) phase.

185 °C from the isotropic melt at 230 °C. After the isothermal formation of the S_{CA} phase at this temperature for a certain period, isotropizaion enthalpy, ΔH_i, was measured at a heating rate of 10 °C min^{-1}. The crystallization behavior from the smectic phase was also examined with a similar procedure. After the sample was annealed at the S_{CA} temperature of 185 °C for 30 min, it was maintained at 140 °C for a certain period for crystallization. The melting enthalpy of the crystal, ΔH_m, was measured at a heating rate of 10 °C min^{-1}.

In Figure 32, ΔH_i and ΔH_m thus determined are plotted against the time of the isothermal transformation, respectively. ΔH_i is relatively constant independent on the transformation time which was varied from 1 to 330 min. This feature of the liquid crystallization is in contrast to that for the crystallization where ΔH_m decreases significantly with a decrease of the crystallization time. Thus, it is likely that the perfect transformation of the isotropic phase to smectic phase takes place in a short period even in the polymeric system. This is reasonable since in the smectic phase the molecules are mobile and can be packed without significant defects although some deformation might be included with respect to the orientation of n- and c-directors. Crystallization does not proceed completely in a short period even if it takes place from the ordered S_{CA} phase. This may be due to the fact that the structural order of the S_{CA} phase is fairly less than that of the crystal. Such characteristic transformations in thermotropic LC polymer system result in the interesting solid morphology in which no isotropic liquid glassy phase is included. In other words, the solid of LC polymer is composed of two phases, LC glass and crystal. This is completely different from that of the conventional polymers which is composed of isotropic liquid glass and crystal.

Because of a very late crystallization, it is possible to prepare the BB-5 solid composed only of the glassy smectic phase by quenching the smectic phase to the room temperature. This is clearly evident from the X-ray photograph as shown in Figure 24, where the pattern characteristic of the mesophase is still observed. DSC thermogram of this sample shows the typical jump of the heat capacity at around 45 °C and dynamic mechanical analysis (DMA) shows the relaxations characteristic to the glass transition as stated in details below.

Figure 33 shows the temperature dependence of the storage tensile modulus (E'), loss modulus (E'') and mechanical loss tangent ($\tan\delta$) for a glassy smectic film of BB-5. Three relaxations can be detected at around 50, −60 and −120 °C, and are designated here as α-, β- and γ-processes, respectively. Since the temperature of α-relaxation corresponds to the glass transition temperature (T_g) detected by DSC, α-relaxation can be connected to the glass transition and attributed to the segmental motion of molecules. The β-process can be connected with the motion of the aromatic part including the ester group.[67,79,80] The γ-process is attributed to local rotation of methylene group commonly observed for polymers containing methylene sequences.[79] These mechanical relaxations are similar to those observed in the isotropic liquid glass of the conventional polymers. The activation energies estimated from the frequency dependence of the relaxation temperature are 75, 35 and 10 kcal mol^{-1} for the α-, β- and γ-relaxations, respectively. Increasing crystallinity by annealing the sample at 140 °C for a certain period (see Figure 32) results in decrease of the loss signal, indicating that the α-process is attributed to a smectic LC glass.

The use of oriented specimens is a further step to understand molecular relaxation. Two smectic LC glassy fibers of BB-5 with different orientations were produced by the two methods of spinning. Fiber A was prepared by drawing the isotropic melt at a high rate of about 1 m sec^{-1}. The X-ray pattern of fiber A shows that the polymer chains lie parallel to the axis and hence that the smectic layers arrange perpendicular to the fiber axis as found in part (a) of Figure 24. Drawing the smectic melt at a low rate of 1 cm sec^{-1} produced fiber B in which the smectic layers lie parallel to the fiber axis, *i.e.*, the polymer chains lie perpendicular to the axis (see part (b) of Figure 24). As stated above, this unusual orientation of fiber B can

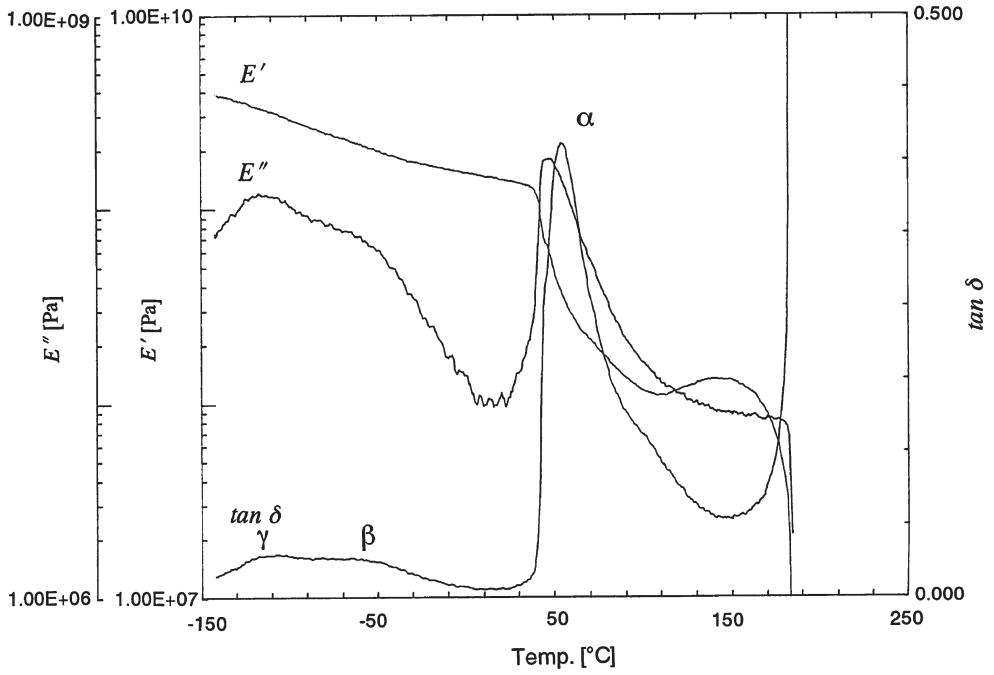

Figure 33. Storage modulus, loss modulus and loss tangent as a function of temperature at 10 Hz for BB-5 specimen quenched from smectic melt.

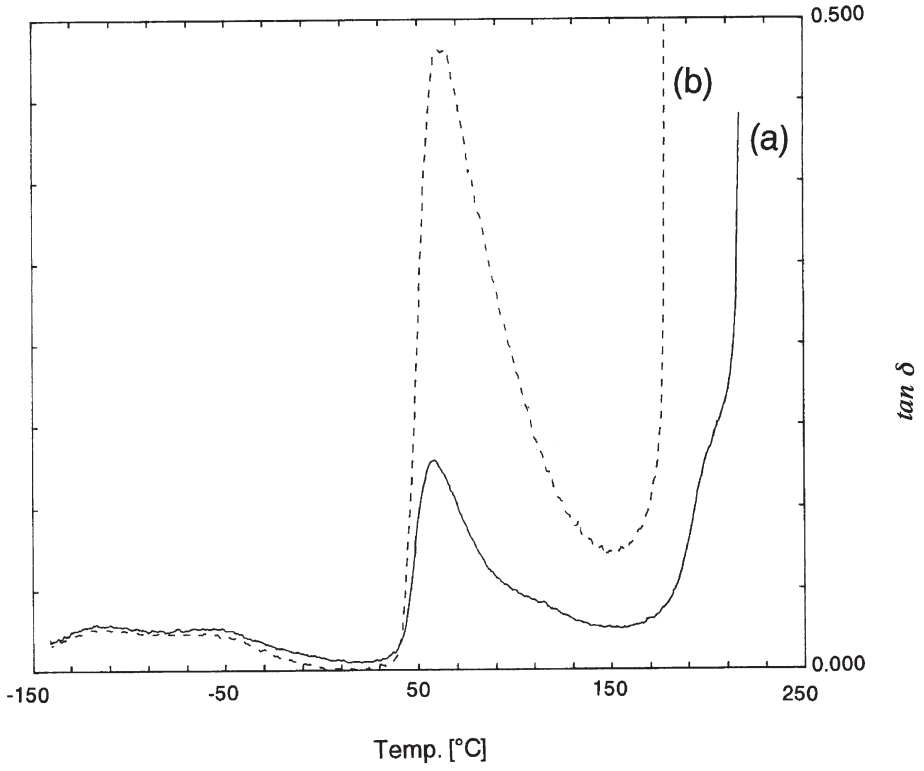

Figure 34. Temperature dependence of loss tangent measured at 10 Hz for the two different BB-5 fibers; (a) solid curve for fiber A and (b) dashed curve for fiber B (refer to Figure 24).

be explained either by mutual slide of chain folded lamellae or by the internal flow of the mesogens within the layer.[16,17,19,22,23] The results of DMA obtained for the two oriented fibers of A and B are shown in Figure 34, where only tan δ are presented because the small cross section of the fibers prevents determining the accurate value of Young's modulus. Considerable mechanical anisotropy with tan δ of fiber B larger than that of fiber A can be seen for the α-relaxation while the intensities of β and γ relaxations are similar.

The ratio of tan δ peak height is around 3. This anisotropy is simply explained according to the layered characteristics of the smectic structure as following. In the S_{CA} phase, the mesogenic groups lie with one-dimensional positional order along the polymer chain axes to form the layers. Along each layer, the center of gravity has no positional order, *i.e.*, the mesogens are laterally packed with liquid-like nature. Hence, the motion of the chain in the direction perpendicular to the layer is restricted while relatively free motion is allowed in the parallel direction.

Anisotropy in mechanical properties is also observed with respect to the terminal flow behavior in the fibers. As seen in Figure 34, the temperature at which the terminal flow takes place so that tan δ diverges to infinity corresponds to T_i (210 °C) for fiber A while it corresponds to T_m (170 °C) for fiber B. This can be also explained in terms of the structural features of smectic phase as mentioned above.

Dependence of Glass Transition Temperature on Carbon Number of Alkyl Spacer

It is interesting to examine how T_g of the LC glass depends on the carbon number of flexible spacer. With respect to this, we first refer to T_g of the isotropic liquid glass observed in the poly(alkylene 2,6-naphthalene dicarboxylate)s (N-*n*) with $n = 5$–12.

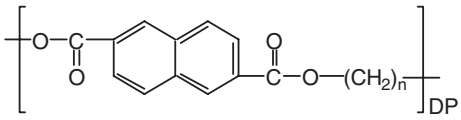

These polyesters form no mesophase so that crystallization takes place directly from the isotropic melt like in the conventional polymers. N-*n* polyesters show three α, β and γ relaxations as observed in BB-5. The temperatures of these relaxations are plotted against *n* by square marks in Figure 35. Here, it should be noted that the β-relaxation temperature was determined with significant error because of the overlapping with α-relaxation. T_α showing odd-even oscillation decreases steadily with an increase of *n*. T_β also decreases with *n* although T_γ is relatively constant at around −130 °C.

These dependences of α, β and γ-relaxation temperatures are interstingly compared with those of the BB-*n* polyesters which are given by circular marks in Figure 35. It must be noted that the BB-*n* polyesters show an unusual variation of T_α on *n*. The LC BB-*n* polyesters with *n* of 5–8 forming the smectic phase show the lower T_α than the non-LC BB-*n* with *n* of 10–12 despite of the higher chain stiffness. This variation is at variance to that observed in N-*n* polyesters, in which T_α decreases steadily with increase of chain flexibility.[80] Since T_α are almost same between non-LC BB-*n* and N-*n* with *n* of 10–12, this

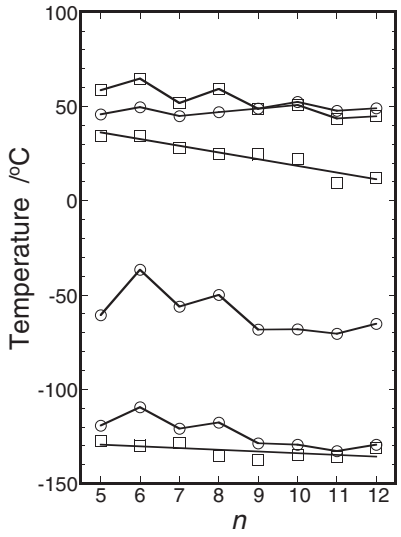

Figure 35. Variation in α-, β- and γ-relaxation temperatures for BB-*n* (circles) and N-*n* (rectangles) polyesters with *n*. Temperatures were determined from the peak of loss modulus, E'', measured at 10 Hz.

anomalous variation can be understood if the smectic LC glass shows the lower T_α than the isotropic liquid glass.

Let us now expand the observation to the copolymers of BB-6-*co*-N-6.

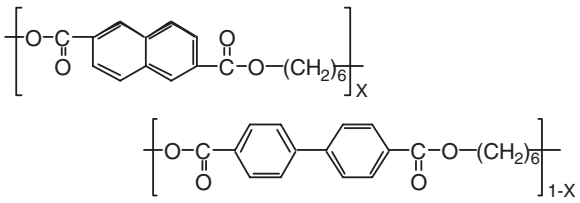

The transition temperatures from the cooling DSC data are plotted against the content of the N-6 unit in Figure 36a. Only copolymers with N-6 contents less than 60% form a S_A phase and so solidify from the S_A phase, while the copolymers with the N-6 contents above 60% solidify directly from isotropic liquid state. As observed in the homopolymers of BB-*n* and N-*n*, the copolymers show up three α-, β- and γ-relaxations. The relaxation temperatures, T_α, T_β and T_γ, are plotted against the molar content of N-6 units in Figure 36b. The glass transition temperature in a copolymer system is related to its composition as described in many cases successfully and simply with the 'Fox-Flory' equation where the glass transition temperature is represented with a continuous function of the volume fractions. In this series of copolymers, T_α remains almost constant around 50 °C up to N-6 content of 60%. For higher N-6 content, T_α rises discontinuously to 70 °C. On comparing this feature with the phase behavior of Figure 36a, one can find that lower T_α is observed for the copolymers forming

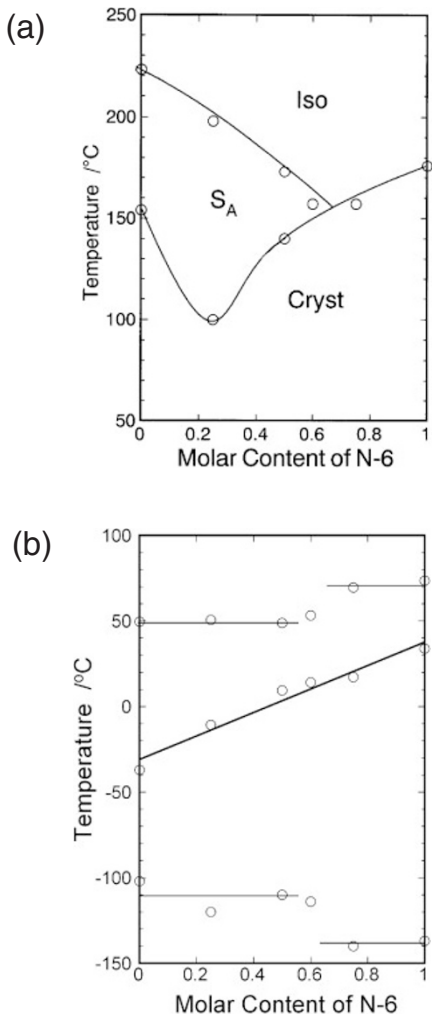

Figure 36. (a) Transition temperatures and phase behavior of BB-6-*co*-N-6 copolyesters. Transition temperatures were determined from the cooling DSC curves measured at a rate of 10 °C min^{-1}. (b) Variation in α-, β- and γ-relaxation temperatures of BB-6-*co*-N-6 copolyesters with the molar content of N-6. Temperatures were determined from the peak of loss modulus, E'', measured at 10 Hz.

the S_A phase. The overall results thus lead to the conclusion that the LC glass shows a lower transition temperature than the isotropic liquid glass.

With respect to the β-relaxation, we find that T_β of N-*n* is fairly higher than that of BB-*n* (see Figure 35). This means that the rotational motion of the naphthalene moiety is more restricted than that of biphenyl moiety. T_β decreases with increase of *n* in both the BB-*n* and N-*n* polymers although T_β of the smectic LC BB-*n* with *n* of 5 to 9 shows some odd-even oscillation. In the BB-6-*co*-N-6 copolymers, as seen in Figure 36b, T_β increases continuously with molar content of N-6 unit, suggesting that the β-relaxation is not closely associated with the structure of the glassy state. T_γ of LC BB-*n* polymers with *n* of 5–9, showing some odd-even oscillation, is relatively higher than that in non-LC N-*n* polymers with identical *n* (see Figure 35). Higher T_γ of the LC glass can be also observed in the copolymer system as found in Figure 36b. T_γ is around −110 °C for the LC copolymers while −140 °C for the non-LC copolymers. This may be caused by extended conformation of polymethylene units in the smectic structures.

Glassy States of Isotopic Liquid and Smectic LC Formed by BB-3(1-Me) Polyester

A main-chain smectic liquid crystalline BB-3(1-Me) polyester is a typical polymer which forms smectic CA liquid crystal (LC) glass and isotropic liquid glass, allowing direct comparison of the properties of two glasses.

Smectic LC glass was obtained by cooling the isotropic liquid to ambient temperature at rates smaller than 1 °C min^{-1}. The resulting solid was opaque and optically anisotropic, and showed an X-ray pattern characteristic to the S_{CA}. Isotropic liquid glass was obtained by rapid cooling of the isotropic melt at rates larger than 50 °C min^{-1}. The solid sample was totally transparent, and its X-ray diffraction pattern included only an amorphous halo. It is noteworthy that in the BB-3(1-Me) polyester, crystallization does not take place at all even if any cooling process is applied. This may be because of packing difficulty due to branched methyl group.

Figure 37 shows DSC thermograms of the two distinct solids measured on heating at a rate of 10 °C min^{-1}. As found in Figure 37a, the smectic LC glass showed a simple thermogram including a jump of the heat capacity at around 81 °C associated to the glass transition and an exothermic peak at 159 °C due to the isotropization of the liquid crystal. The isotropic

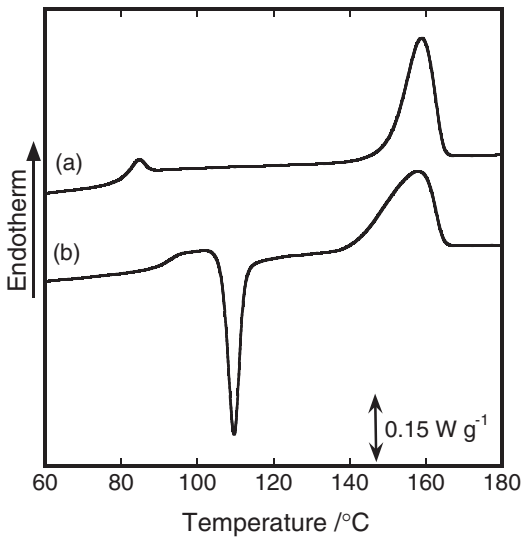

Figure 37. DSC thermograms for the BB-3(1-Me) polyester cooled from the isotropic liquid state to ambient temperature at a rate of 1 °C min^{-1} (a), and 100 °C min^{-1} (b).

liquid glass showed a somewhat complex thermogram. The DSC thermogram shown in Figure 37b includes a step at 93 °C associated with the glass transition of the isotropic liquid, a sharp exothermic peak at 110 °C and finally an endothermic peak at 159 °C. The exothermic peak following the glass transition is due to the liquid crystallization of the relaxed isotropic liquid glass, and the final endothermic peak at 159 °C is attributed to the isotropization of the resulting smectic LC. The difference in the glass transition temperature (T_g) is significant between the two types of glasses: T_g for the isotropic liquid glass (T_g^{iso}) is 12 °C higher than T_g for the smectic LC glass (T_g^{LC}). This trend coincides with that observed in the previous part of this section. A similar result has been reported for main-chain liquid crystalline polymers which can form these two glassy states.[69,70,76,77]

To cralify in more detail thermodynamic properties, specific heat was measured by the temperature-modulated DSC (TMDSC) method.[81,82] Temperature dependences of C_P' and C_P'' determined at a frequency of 1.7×10^{-2} Hz are shown in Figures 38a and 38b, respectively. C_P' of the two glasses are comparable to each other, showing that similar molecular motion takes place in the glassy states. In the glass transition, C_P' and C_P'' show a jump and a peak, respectively.

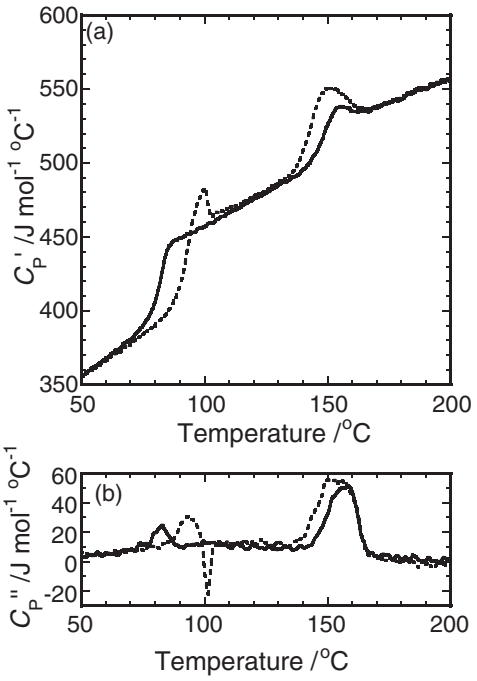

Figure 38. Temperature dependence of storage heat capacity C_P' (a) and loss heat capacity C_P'' (b) determined by temperature modulated DSC for the BB-3(1-Me) polyester cooled from the isotropic liquid state to ambient temperature at a rate of 1 °C min^{-1} (solid curve) and 100 °C min^{-1} (dotted curve). The temperature modulation amplitude, averaged heating rate and periodic time were 0.5 °C, 1 °C min^{-1} and 60 s, respectively.

TMDSC data clearly show that T_g^{iso} (92 °C) is higher than T_g^{LC} (81 °C), as found in the conventional DSC thermograms (see Figure 37). The corresponding increase in C_P' determines ΔC_P in the glass transition more accurately than the conventional DSC thermogram, because TMDSC is not influenced by the enthalpy relaxation endotherm overlapping with glass transition.[65,66] ΔC_P thus estimated were 78.5 J mol^{-1} K^{-1} and 50.1 J mol^{-1} K^{-1} for the isotropic liquid glass and the smectic LC glass, respectively. The difference in ΔC_P reflects the difference in molecular motion between the isotropic liquid and the smectic LC. In the C_P' curve of the isotropic liquid glass, the jump is followed by a drop, and the value becomes equal to that of the smectic LC. This drop is thus attributed to the liquid crystallization of the relaxed isotropic liquid glass, but the corresponding exothermic peak observed in the conventional DSC thermogram (Figure 37b) is not found in the C_P' curve in Figure 38a. This is reasonable since the TMDSC is not influenced by thermal events arising from kinetic process such as the liquid crystallization.

TMDSC thermograms give temperature dependence of the heat capacities of the smectic LC and the isotropic liquid as well as the two glassy states. The temperature dependence of C_P in the measurement temperature range is expressed as

$$C_P = a + bT, \tag{2}$$

where a and b are the constants determined with temperature dependence of C_p'. The enthalpy in each state was obtained by integration of eq 2 to estimate the enthalpy-temperature relationship.

$$H = \int C_P dT = aT + bT^2/2 + c. \tag{3}$$

Here, c is the arbitrary constant determined by taking account of continuity in the enthalpy at the glass transition and the enthalpy difference at the isotropic liquid-smectic LC transition and by setting the reference point as the enthalpy of the liquid = 0 J mol^{-1} at 0 K. Figure 39 shows temperature dependence of the enthalpy estimated for each state by eq 3. Quantitative accuracy of the enthalpy-temperature relationship can be confirmed by comparison of the difference in the enthalpy between the isotropic liquid and the smectic LC at 110 °C (3.25 kJ mol^{-1}, see Figure 39) with the enthalpy change in the liquid crystallization taking place at 110 °C on heating the isotropic liquid glass (3.11 kJ mol^{-1}, see Figure 39b). In the enthalpy-temperature diagram, the enthalpy at T_g for the smectic LC is smaller than that for the isotropic liquid, and that the difference between them ($\Delta H_g = 8.02$ kJ mol^{-1}) is about two times larger than the enthalpy change at the isotropic – smectic LC transition

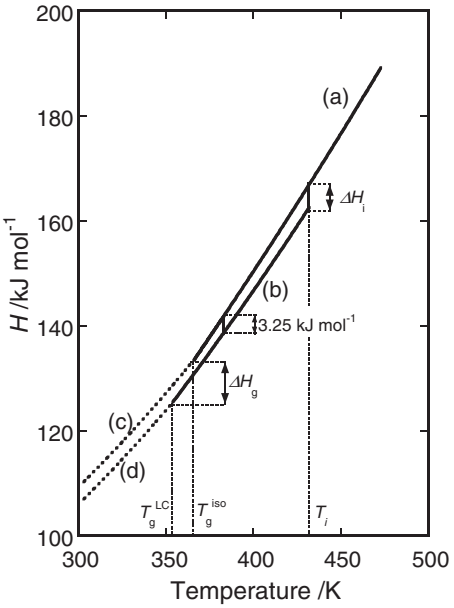

Figure 39. Enthalpy-temperature relationship of the BB-3(1-Me) in the isotropic liquid state (a), the smectic LC state (b), the isotropic liquid glass state (c), and the smectic LC glass state (d). Enthalpy was calculated by integration of the heat capacity evaluated by TMDSC (see eq 3). Transition temperatures, T_i, T_g^{iso} and T_g^{LC}, and isotropization enthalpy, ΔH_i, are based on the conventional DSC thermograms in Figure 37.

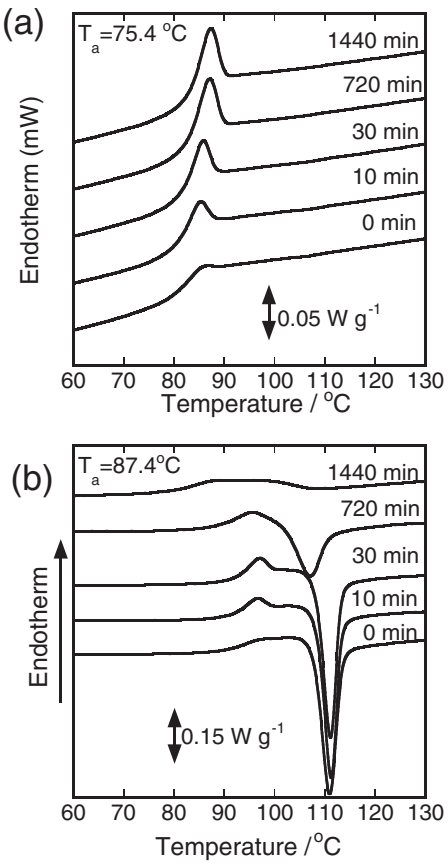

Figure 40. DSC thermograms measured by heating the smectic LC glass (a) and isotropic liquid glass (b) stored at 75.4 °C and 87.4 °C, respectively, for the period indicated in the figure. The heating rate was 10 °C min^{-1}.

($\Delta H_i = 4.47\,\mathrm{kJ\,mol^{-1}}$). On the assumption that enthalpy is proportional to specific volume, this quantitative result is related to a supposition submitted by Zachmann *et al.*[69] to explain the lower T_g of the LC glass: the critical volume at T_g for the LC is smaller than that for the isotropic liquid, and the difference between them is larger than the volume change at the isotropic-LC transition.

Two Glass Transitions Observed in Isotropic Liquid of Main-Chain LC Polymer

The two glasses undergo enthalpy relaxation, which is apparent as the endotherm peak appearing immediately after the glass transition in the heating DSC thermogram as seen in Figure 40a. Extent of this relaxation process can be detected by growth of the endothermic peak measured for the glassy solid stored at certain temperature, T_a, below T_g for prolonged aging period. The endothermic values were determined by subtracting the DSC curve for the un-aged glassy sample from that for the aged sample, and are plotted against the aging period in Figure 41. Aging time dependence of the endothermic value is well fitted to Cowie-Ferguson equation[83]

$$\Delta H(t) = \Delta H_\infty (1 - e^{-(t/\tau)^\beta}), \qquad (4)$$

for both these glasses as seen in Figure 41. Thus, we can determine kinetic parameters of average relaxation time, τ and measure of width of the underlying relaxation spectrum, β. Here ΔH_∞ is comparable to the value estimated by a simple relationship of $\Delta H_\infty = \Delta C_P(T_g - T)$. The relaxation rates depend on extent of undercooling from the glass transition temperature, while β is not significantly dependent on the aging temperature nor the type of the glassy state.

In Figure 42 the reciprocal of τ (τ^{-1}) is plotted against the reciprocal of the aging temperature in unit of K^{-1}. Temperature dependence of τ is usually portrayed by Vogel-Fulcher-Tamman (VFT) relationship:

$$\tau = A \exp \frac{Q}{T - T_0}, \qquad (5)$$

where A and T_0 are prefactor and ideal glass temperature, respectively. VFT equation expects a non-Arrhenius relationship between τ^{-1} and $1/T_a$ where τ^{-1} decreases more rapidly with increment in T_a^{-1} to give a single glass temperature, T_0. Such a relationship is found for the smectic LC to give T_0^{LC} of 343 K (see Figure 42). For the isotropic liquid, however, the decrease in τ^{-1} takes place in two steps; the decrease of τ^{-1} in T_a^{-1} larger than $2.775 \times 10^{-3}\,\mathrm{K^{-1}}$ is less

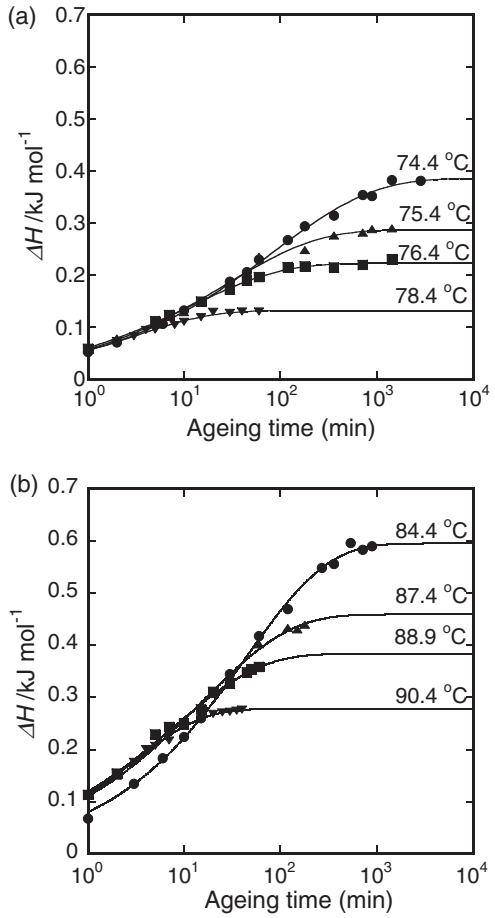

Figure 41. Aging time dependence of the enthalpy relaxation endotherm for the smectic LC glass (a) and the isotropic liquid glass (b) at the temperature indicated in the figure. Solid curve shows the validity of Cowie-Ferguson equation.

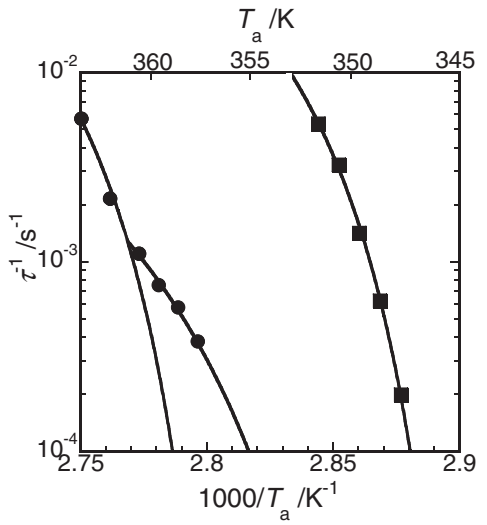

Figure 42. Arrhenius plots of enthalpy relaxation time in the isotropic liquid (circle) and the smectic LC (square). The solid curve shows validity of VFT description.

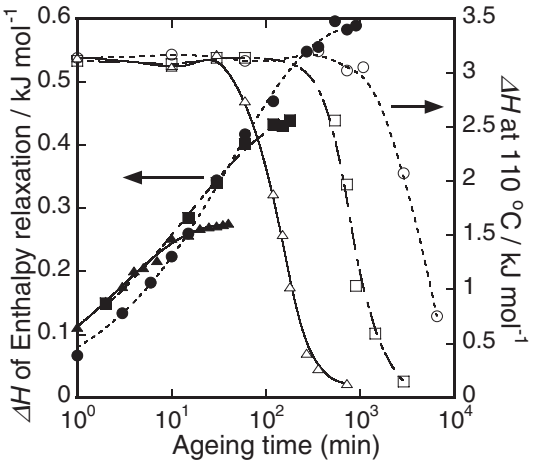

Figure 43. Aging time dependence of the enthalpy of the exothermic peak at 110 °C attributed to the liquid crystallization (open symbols). The data shown by circle, square and triangle are collected at aging temperatures of 84.4 °C, 87.4 °C and 90.4 °C, respectively. Aging time dependences of the enthalpy relaxation endotherm of isotropic liquid glass (closed symbols), the same in Figure 41b, are also given for a comparison.

than that in smaller T_a^{-1}. The data at T_a^{-1} larger and smaller than $2.775 \times 10^{-3}\,K^{-1}$ give T_{0L}^{iso} of 343 K and T_{0H}^{iso} of 353 K, respectively. T_{0L}^{iso} is 10 K lower than T_{0H}^{iso} and is interestingly equal to T_0^{LC}.

In addition to the enthalpy relaxation, as found in Figure 40b, aging of the isotropic liquid glass also decreases the exothermic value at 110 °C, showing that the liquid crystallization takes place simultaneously in the relaxed isotropic liquid glass. In Figure 43, the enthalpy values of the liquid crystallization are plotted against ageing time and compared with the enthalpy values of the enthalpy relaxation. The isotropic liquid glass clearly transforms to the smectic LC after completion of the enthalpy relaxation.

Liquid crystallization was followed with the fraction conversion (X_t), which was estimated from decrease in the area of the exothermic peak due to the liquid crystallization of the unconverted isotropic liquid in the DSC thermograms. We take the inverse of the time at which X_t is 50% to represent the measure of the transition rate, $t_{1/2}^{-1}$. The transition rate shows the VFT type temperature dependence as shown in Figure 44, giving two glass temperatures of 344 K and 355 K. These temperatures approximate T_{0H}^{iso} and T_{0L}^{iso} estimated though the enthalpy relaxation rate of the isotropic liquid glass. The appearance of two glass transitions in the isotropic liquid and the coincidence between T_{0L}^{iso} and T_0^{LC} thus seem more than casual ones.

Two ideal glass temperatures of isotropic liquid of LC material are discussed in recent works on glass transition, by extension of a mode coupling theory (MCT) to hard ellipsoids.[84] According to this theory,

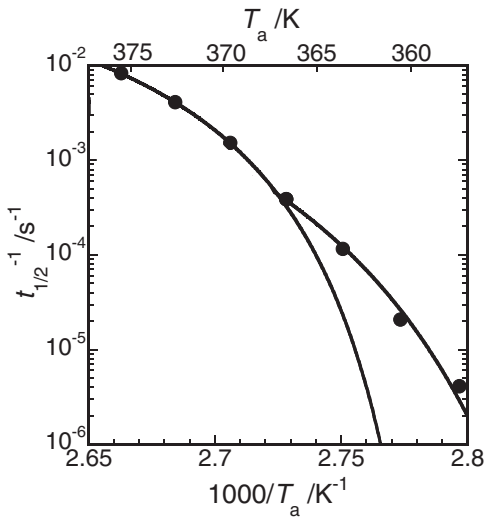

Figure 44. Arrhenius plot of the liquid crystallization rate. The solid curve shows the validity of VFT description.

the ellipsoids with aspect ratio greater than 2.5 (calamitic mesogens) freeze their orientational degree of freedom, and remaining translational degree of freedom attaches still liquid like nature to some extent to the system. Temperature scaling analysis for optical heterodyne detected optical Kerr effect data for low molecular weight nematic LC materials have represented two glass transitions of the isotopic liquid.[85] The two ideal glass temperatures found in this study may thus be understood by the same way: $T_{0H}{}^{iso}$ is attributed to the freezing of molecular orientation fluctuation while $T_{0L}{}^{iso}$ to the freezing of molecular translation motions. The glass transition in the smectic LC is attributable to the freezing of translational molecular motion within the layer.[18,24] This seems to be the reason why $T_0{}^{LC}$ corresponds to $T_{0L}{}^{iso}$.

REFERENCES AND NOTES

1. W. R. Krigbaum and J. Watanabe, *Polymer*, **24**, 1299 (1983).
2. J. Watanabe and M. Hayashi, *Macromolecules*, **21**, 278 (1988).
3. J. Watanabe and M. Hayashi, *Macromolecules*, **22**, 4083 (1989).
4. H. Takezoe, A. Fukuda, A. Ikeda, Y. Takanishi, T. Uemoto, H. Iwane, M. Hara, K. Itoh, and J. Watanabe, *Ferroelectrics*, **122**, 167 (1991).
5. J. Watanabe, M. Hayashi, S. Kinoshita, and T. Niori, *Polym. J.*, **24**, 597 (1992).
6. J. Watanabe and S. Kinoshita, *J. Phys. II (France)*, **2**, 1273 (1992).
7. Y. Takanishi, H. Takezoe, A. Fukuda, J. Watanabe, and H. Komura, *J. Mater. Chem.*, **2**, 71 (1992).
8. Y. Takanishi, H. Takezoe, A. Fukuda, and J. Watanabe, *Phys. Rev. B*, **45**, 7684 (1992).
9. J. Watanabe, H. Komura, and T. Niori, *Liq. Cryst.*, **13**, 455 (1993).
10. Y. Nakata and J. Watanabe, *J. Mater. Chem.*, **4**, 578 (1994).
11. Y. Nakata, K. Shimizu, and J. Watanabe, *J. Phys. II (France)*, **4**, 581 (1994).
12. J. Watanabe, M. Hayashi, A. Morita, and T. Niori, *Mol. Cryst. Liq. Cryst.*, **254**, 221 (1994).
13. Y. Nakata and J. Watanabe, *High Performance Polym.*, **7**, 377 (1995).
14. a) J. Watanabe, M. Hayashi, A. Atsushi, and M. Tokita, *Macromolecules*, **28**, 8073 (1995).
    b) J. Watanabe, M. Hayashi, and M. Tokita, *React. Funct. Polym.*, **30**, 191 (1996).
15. J. Watanabe, T. Niori, and S. Adachi, *Liq. Cryst.*, **19**, 139 (1995).
16. M. Tokita, T. Takahashi, M. Hayashi, and J. Watanabe, *Macromolecules*, **29**, 1345 (1996).
17. M. Tokita, K. Osada, and J. Watanabe, *Liq. Cryst.*, **22**, 453 (1997).
18. M. Tokita, K. Osada, and J. Watanabe, *Polym. J.*, **30**, 589 (1998).
19. M. Tokita, K. Osada, S. Kawauchi, and J. Watanabe, *Polym. J.*, **30**, 687 (1998).
20. M. Tokita, K. Osada, and J. Watanabe, *Liq. Cryst.*, **24**, 477 (1998).
21. M. Tokita, K. Tokunaga, S. Funaoka, K. Osada, and J. Watanabe, *Macromolecules*, **37**, 2527 (2004).
22. K. Osada, M. Koike, H. Tagawa, S. Funaoka, M. Tokita, and J. Watanabe, *Macromolecules*, **38**, 7337 (2005).
23. M. Tokita, S. Funaoka, and J. Watanabe, *Macromolecules*, **37**, 9916 (2004).
24. K. Osada, M. Koike, H. Tagawa, M. Tokita, and J. Watanabe, *Macromol. Chem. Phys.*, **205**, 1051 (2004).
25. A. Abe, *Macromolecules*, **17**, 2280 (1984).
26. In the previous reports,[2–9] this phase has been termed S_{C2} phase, but S_{C2} is a confusing notation in the context of the nomenclature described in low molar mass systems. For this reason, we adopted the notation of S_{CA} which has been termed for the same type of smectic phase in low molar mass system by Fukuda, *et al.* [*Jpn. J. Appl. Phys.*, **28**, L1265 (1989)].
27. G. W. Gray and J. W. Goodby, "Smectic Liquid Crystals," Leonald Hill, Glasgow and London, 1984.
28. W. F. Harris, *Philos. Mag.*, **22**, 949 (1970).
29. Michelson, D. Cabid, and L. Benguigui, *J. Phys. (France)*, **38**, 961 (1977).
30. D. W. Berreman, *Mol. Cryst. Liq. Cryst.*, **22**, 175 (1973).
31. G. S. Chilaya, S. N. Aronishidze, and M. N. Kushnirenko, *Mol. Cryst. Liq. Cryst. (Lett.)*, **82**, 281 (1982).
32. R. G. Petscheck and K. M. Wiefling, *Phys. Rev. Lett.*, **59**, 343 (1987).
33. International Table for X-ray Crystallography Vol. I, Birmingham, Kynoch Press, 1959, p. 208; it should be noted here that this space group is essentially different from that of the S_{CA} phase which is analogous to the crystallographic D_{2h}.
34. G. Sigaud, F. Hardouin, M. F. Achard, and A. M. Levelut, *J. Phys. (France)*, **42**, 107 (1981).
35. J. Prost and P. Barois, *J. Chem. Phys.*, **80**, 65 (1983).

36. J. Prost, *Adv. Phys.*, **33**, 1 (1984).
37. Y. Nakata and J. Watanabe, *Polym. J.*, **29**, 193 (1997).
38. J. Watanabe, T. Niori, S. W. Choi, Y. Takanishi, and H. Takezoe, *Jpn. J. Appl. Phys.*, **37**, L401 (1998).
39. T. Niori, T. Sekine, J. Watanabe, T. Furukawa, and H. Takezoe, *J. Mater. Chem.*, **7**, 1231 (1996).
40. J. Watanabe, T. Niori, T. Sekine, T. Furukawa, and H. Takezoe, *J. Mater. Chem.*, **7**, 1307 (1997).
41. J. Watanabe, T. Sekine, Y. Takanishi, T. Niori, and H. Takezoe, *Jpn. J. Appl. Phys.*, **36**, L1201 (1997).
42. J. Watanabe, T. Sekine, T. Niori, S. W. Choi, M. Sone, Y. Takanishi, T. Niori, and H. Takezoe, *Jpn. J. Appl. Phys.*, **36**, 6455 (1997).
43. J. Thisayukta, S. Kawauchi, H. Takezoe, and J. Watanabe, *Jpn. J. Appl. Phys.*, **40**, 3277 (2001).
44. J. Thisayukta, Y. Nakayama, S. Kawauchi, H. Takezoe, and J. Watanabe, *J. Am. Chem. Soc.*, **122**, 7441 (2000).
45. J. Thisayukta, H. Niwano, H. Takezoe, and J. Watanabe, *J. Am. Chem. Soc.*, **124**, 3354 (2002).
46. D. A. Coleman, J. Fernsler, N. Chattham, M. Nakata, Y. Takanishi, D. R. Link, R.-F. Shao, W. G. Jang, J. E. Maclennan, E. Körblova, O. Mondain, C. Boyer, W. Weissflog, G. Pelzl, L.-C. Chien, D. M. Walba, J. Zasadzinski, J. Watanabe, H. Takezoe, and N. A. Clark, *Science*, **301**, 1204 (2003).
47. P. G. de Gennes, in "Polymer Liquid Crystals," A. Cifferri, W. R. Krigbaum, and R. B. Mayer, Ed., Academic Press, New York, 1982, p 124.
48. X. J. Wang and M. Warner, *Phys. A*, **19**, 2215 (1986).
49. D. R. M. Williams and M. Warner, *J. Phys. France*, **51**, 317 (1990).
50. J. F. D'Allest, P. Sixou, A. Blumstein, and R. B. Blumstein, *Mol. Cryst. Liq. Cryst.*, **155**, 581 (1988).
51. V. Arrighi, J. S. Higgins, R. A. Weiss, and A. L. Cimecioglu, *Macromolecules*, **25**, 5297 (1992).
52. M. H. Li, A. Brulet, P. Davidson, P. Keller, and J. P. Cotton, *Phys. Rev. Lett.*, **70**, 2293 (1993).
53. M. H. Li, A. Brulet, J. P. Cotton, P. Davidson, C. Strazielle, and P. Keller, *J. Phys. II (France)*, **4**, 1843 (1994).
54. T. Takahashi and F. Nagata, *J. Macromol. Sci. Phys.*, **B28**, 34 (1989).
55. E. W. Fisher and G. F. Schmidt, *Angew. Chem., Int. Ed.*, **1**, 488 (1962).
56. P. J. Barham, R. H. Chivers, A. Keller, J. Martines-Salazar, and S. J. Organ, *J. Mater. Sci.*, **20**, 1625 (1985).
57. S. P. Church, V. L. Patel, N. Khan, and Z. Bashir, *Mol. Cryst. Liq. Cryst.*, **289**, 25 (1996).
58. M. Leland, Z. Wu, C. Chhajer, R.-M. Ho, S. Z. D. Cheng, A. Keller, and H. R. Kricheldorf, *Macromolecules*, **30**, 5249 (1997).
59. P. Bello, A. Bello, and V. Lorenzo, *Polymer*, **42**, 4449 (2001).
60. A. Martinz-Gomez, J. M. Perena, V. Lorenzo, A. Bello, and E. Perez, *Macromolecules*, **36**, 5798 (2003).
61. K. A. Koppi, M. Tirrell, F. S. Bates, F. K. Almdal, and R. H. Colby, *J. Phys. II (France)*, **2**, 1941 (1992).
62. R. Bruinsma and Y. Rabin, *Phys. Rev.*, **45**, 994 (1992).
63. P. G. de Gennes and J. Prost, "The Physics of Liquid Crystals," 2nd ed., Oxford University Press., New York, 1993.
64. M. Tokita, H. Tagawa, S. Funaoka, H. Niwano, K. Osada, and J. Watanabe, *Jpn. J. Appl. Phys.*, **45**, 1729 (2006).
65. K. Tsuji, M. Sorai, and S. Seki, *Bull. Chem. Soc. Jpn.*, **44**, 1452 (1971).
66. G. P. Johari and J. W. Goodby, *J. Chem. Phys.*, **77**, 5165 (1982).
67. V. Frosoni, S. De Petris, E. Chiellini, G. Galli, and R. W. Lenz, *Mol. Cryst. Liq. Cryst.*, **98**, 223 (1983).
68. B. Wunderlich and J. Grebowicz, *Adv. Polym. Sci.*, **60/61**, 1 (1984).
69. D. Chen and H. G. Zachmann, *Polymer*, **32**, 1612 (1991).
70. O. Ahumada, T. A. Ezquerra, A. Nogales, F. J. Baltà-Colleja, and H. G. Zachmann, *Macromolecules*, **29**, 5002 (1996).
71. W. Welder, D. Demus, H. Zaschke, K. Mohr, W. Schäfer, and W. Weissflog, *J. Mater. Chem.*, **1**, 347 (1991).
72. W. Welder, P. Hartmann, U. Bakowsky, S. Diele, and D. Demus, *J. Mater. Chem.*, **2**, 1195 (1992).
73. Y. Gonzalez, B. Palacios, M. A. Pérez Jubindo, M. Rosario de la Fuente, and José Luis Serrano, *Phys. Rev. E.*, **52**, R5764 (1995).
74. B. Palacios, M. R. De La Fuente, M. A. Pérez Jubindo, and M. B. Ros, *Liq. Cryst.*, **23**, 349 (1997).
75. A. del Campo, T. A. Ezquerra, G. Wilbert, M. Paßmann, and R. Zentel, *Macromol. Chem. Phys.*, **203**, 2089 (2002).
76. A. del Campo, A. Bello, E. Pérez, A. García-Bernabé, and R. Díaz Calleja, *Macromol. Chem. Phys.*, **203**, 2508 (2002).
77. A. García-Bernabé, R. Díaz Calleja, M. J. Sanchis, A. del Campo, A. Bello, and E. Pérez, *Polymer*, **45**, 1533 (2004).
78. S. H. Chen, H. M. Phillip Chen, Y. Geng, S. D. Jacob, K. L. Marchell, and T. N. Blanton, *Adv. Mater.*, **15**, 1061 (2003).
79. G. Farrow, J. McIntosh, and I. M. Ward, *Makromol. Chem.*, **38**, 147 (1960).
80. N. G. McCrum, B. E. Read, and G. Williams, "Anelastic and Dielectric Effects in Polymeric Solids," Wiley, New York, 1967.
81. J. E. K. Schawe, *Thermochim. Acta*, **260**, 1 (1995).
82. M. Reading, *Trends Polym. Sci.*, **1**, 248 (1993).
83. A. Brunacci, J. M. G. Cowie, R. Ferguson, and I. J. McEwen, *Polymer*, **38**, 865 (1997).
84. M. Letz, R. Schilling, and A. Latz, *Phys. Rev. E.*, **62**, 5173 (2000).
85. H. Cang, J. Li, V. N. Novikov, and M. D. Fayer, *J. Chem. Phys.*, **119**, 10421 (2003).

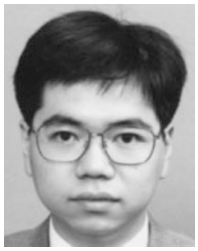

Masatoshi Tokita, born in 1971 (Tokyo, Japan), received his B.S. in 1994 and Ph.D. in 1999 (Tokyo Institute of Technology). He worked as an assistant professor at Graduate School of Bio-Application and Systems Engineering in Tokyo University of Agriculture and Technology from 1997 to 2000. Since July 2000, he is an assistant professor at Department of Organic and Polymeric Materials in Tokyo Institute of Technology. His research interest is the structure and dynamics of polymer liquid crystals.

Junji Watanabe, born in 1948 (Ehime, Japan), received his B.S. in 1970 and Ph. D. in 1976 (Tokyo Institute of Technology). Since 1976, he worked as assistant professor, associate professor and full professor at Department of Polymer Chemistry in Tokyo Institute of Technology. His research interest is the structure and properties of polymer liquid crystals based on polypeptides, polysaccharides, polysilanes, and polyesters.